Form-finding of shell structures generated from physical models

Li, Qingpeng; Su, Y.; Wu, Y.; Borgart, Andrew; Rots, Jan

DOI
10.1177/0266351117696577

Publication date
2017

Document Version
Final published version

Published in
International Journal of Space Structures

Citation (APA)
Li, Q., Su, Y., Wu, Y., Borgart, A., & Rots, J. (2017). Form-finding of shell structures generated from physical models. *International Journal of Space Structures*, *32*(1), 11-33. https://doi.org/10.1177/0266351117696577

International Journal of
SPACE
STRUCTURES

Article

Form-finding of shell structures generated from physical models

International Journal of Space Structures
2017, Vol. 32(1) 11–33

DOI: 10.1177/0266351117696577
journals.sagepub.com/home/sps
SAGE

Qingpeng Li[1,2], Yan Su[1], Yue Wu[1], Andrew Borgart[2] and Jan G Rots[2]

Abstract

Vector form intrinsic finite element is a recently developed and promising numerical method for the analysis of complicated structural behavior. Taking the cable-link element as example, the framework of the vector form intrinsic finite element is explained first. Based on this, a constant strain triangle element is introduced, and relevant required equations are deduced. Subsequently, the vector form intrinsic finite element is successfully applied to carry out form-finding of shells generated from physical models, such as hanging models, tension models, and pneumatic models. In addition, the resulting geometries are analyzed with finite element method, thus demonstrating that a dominant membrane stress distribution arises when the shell is subjected to gravitational loading.

Keywords

form-finding, physical models, shell structures, structural analysis, vector form intrinsic finite element

Introduction

Background and related research

For a shell structure, the geometric shape plays an important role in its structural efficiency. The stress state occurring in a shell depends strongly on its three-dimensional shape, and the ideal stress state for shells is pure compression. Therefore, to obtain a structurally efficient shell, its shape should depend on the flow of forces, and vice versa, its design requires a process of form-finding. For form-finding of shells, physical models and many numerical methods have been developed by researchers, engineers, architects, or contractors over the past several decades.

In the pre-computer age, physical models based on the "form follows force" principle were widely used to design or construct shells. Nowadays, in most cases, physical models are being used in teaching activities to reveal the mechanical principles and in the construction process as moulds. As form-finding means, physical models are made of small pieces of flexible membranes or fabrics subject to certain loads and boundary conditions, and after evaluating and scaling them, efficient shapes of shells can be obtained. As moulds for construction, referring to pneumatic physical models in this article, they are made of flexible membranes but with real sizes, and afterward they would be covered with building materials. Based on their different manufacturing methods, these physical models can be divided into three groups.

Hanging models. Based on its structural principle, the form of a hanging model is self-forming and capable of transferring its self-weight and area load solely by means of tension, and when it is turned upside down, a pure compression model arises. Heinz Isler (1926–2009)[1,2] developed a number of hanging models to determine suitable shapes of concrete shells, and Figure 1 shows one case with such a structure. In addition, Frei Otto (1925–2015)[3] used hanging chain models for designing grid

[1]Harbin Institute of Technology, P.R. China
[2]Delft University of Technology, The Netherlands

Corresponding author:
Yue Wu, Key Lab of Structures Dynamic Behavior and Control of China Ministry of Education, Harbin Institute of Technology, Harbin 150090, P.R. China.
Email: wuyue_2000@163.com

Figure 1. Deitingen Service Station, Switzerland, 1968 (https://structurae.net/structures/deitingen-service-station).

Figure 2. Roof for Multihalle in Mannheim, Germany, 1975 (https://www.pinterest.com/pin/457045062154696404/).

shells, and one example is the roof for the Multihalle in Mannheim shown in Figure 2.

Tension models. These models, which are made of soap film or gauze, aim to find the equilibrium shape of a minimal surface between preset boundaries. They represent a highly significant tool for exploring the shapes of tent constructions. However, tension models were also used for form-finding of shells. Frei Otto[3] applied this kind of model in the design of the Stuttgart train station, demonstrating the formal and structural novelty which derives from experiments with minimal surfaces, and Figure 3 shows the suspension model for form-finding of the arches for this project. In addition, Sergio Musmeci (1926–1981)[4] designed the shell-supported slabs using physical models, and Figure 4 shows the Basento Viaduct in Potenza.

Pneumatic models. For these models, the soap film or a piece of membrane (air tight or allowing very little air through) is blown in a certain shape possibly with a closed preset boundary, and the overpressure inside then forms an equilibrium shape. Pneumatic models can be adopted to determine the efficient shape of shells, and they can also

Figure 3. Suspension model for form-finding of the arches of the new train station in Stuttgart, Germany, 2000 (https://www.pinterest.com/pin/317011261243639594/).

Figure 4. Basento Viaduct in Potenza, Italy, 1974 (https://www.pinterest.com/pin/481111172670145006/).

be used as moulds for construction. Pneumatic models were also favored by Heinz Isler[1,2] to design concrete shells, and one example with such structure is shown in Figure 5. As molds for construction, pneumatic models were extensively used by Bini[5] to design and construct reinforced concrete thin-shells (Figure 6), and were also applied by Kokawa[6] to design and construct ice-shells (Figure 7).

From the above introduction, it can be observed that each group of physical models represents a typical type of static force equilibrium which obeys the "form follows force" principle. However, all these three groups of physical models maintain a pure tension state subject to certain loads and boundary conditions. When they are used as shapes of shells after some required measures (e.g. inversion, scaling proportionally, section design) and construction, the shells will maintain a high structural efficiency.

Since the 1960s, with the development of analysis theories and computer techniques, numerical form-finding methods have become the most important means to generate structural forms of shells. These methods generate ideal shapes that are the results of stable force equilibrium.

Figure 5. COOP storage and distribution center, Wangen, Switzerland, 1960[2].

Figure 6. One Binishell in Ku-ring-gai High School (http://www.khs82.com/dbpage.php?pg=khsphotos).

Figure 7. An Ice Dome at Tomamu in Hokkaido, Japan, 2001[6].

Among these many numerical methods, Dynamic Relaxation method[7], Force Density method[8,9], finite element based methods[10], structural optimization based methods[11], Vector Form Intrinsic Finite Element (VFIFE) method[12–14], and Thrust Network Analysis method[15] can be used to solve form-finding problems for cable or membrane structures and thus for shells. To know more about these numerical methods, Vizotto[16] gave a more detailed summary of various form-finding methods and their applications, Veenendaal and Block[17] conducted a comprehensive technical comparison of various form-finding methods, and an extensive overview of various form-finding techniques for shells is given in the book *Shell Structures for Architecture: Form Finding and Optimization* edited by Adriaenssens et al[18].

Development of the VFIFE method

The VFIFE method is a relatively new numerical analysis method proposed by Ting et al.[12,13] and Shih et al[14]. Other than the traditional numerical analysis methods which are based on continuum mechanics and variational principles, VFIFE is based on point value description and the vector mechanics theory. With the description of point values and path units, VFIFE describes the structural system composed of particles whose motions are determined by Newton's second law. During the calculation procedure, there is no need to integrate the structural stiffness matrix, and it can increase (or decrease) elements or change any property of the structural system. Therefore, VFIFE has a remarkable predominance in nonlinear problems and complex behaviors of structures compared with the traditional numerical analysis methods.

Recently, many scholars[19–23] are conducting research using VFIFE in the field of complicated behavior analysis of structures, including geometric nonlinearity, material nonlinearity, mechanism motion, dynamic responses, buckling or wrinkles failure, and so forth. VFIFE has showed its great benefit in these fields. Moreover, based on VFIFE, Luo et al.[24] and Yang et al.[25] proposed a new method called the Finite Particle method to study the structural behavior analysis and form-finding of spatial structures.

VFIFE can be also used in the field of form-finding research. In this article, VFIFE is introduced to carry out form-finding of shells inspired by the three types of physical models.

Outline of this article

Taking the cable-link element as example, the basic concepts and procedure of VFIFE are explained in the first two parts of section "The VFIFE method". Subsequently, according to the above, a constant strain triangle element based on VFIFE is introduced, and relevant required equations are deduced.

In section "Numerical form-finding of shell structures", using VFIFE, form-finding of shells which are generated from hanging models, tension models, and pneumatic models is discussed. One numerical example is presented in each kind of form-finding. Moreover, in order to verify the capability of VFIFE in finding optimal structural shapes for shells, structural analysis of these form-found shells is conducted, which present that a dominant

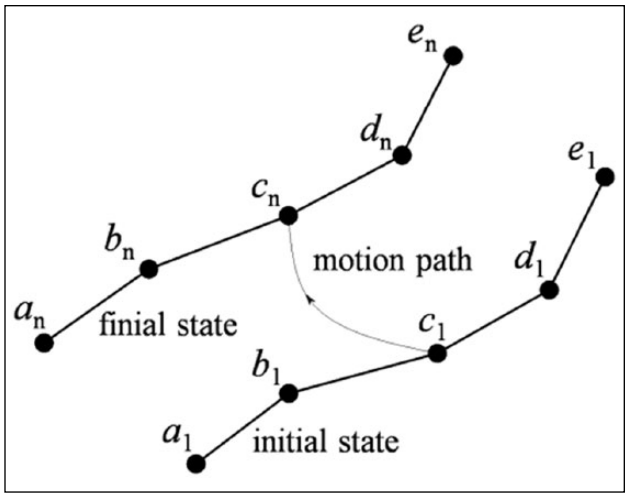

Figure 8. Discretion of the structural system.

membrane stress state arises when the shell is subject to gravitational loading while out-of-plane stresses remain comparatively low.

Finally, some main conclusions concerning form-finding of shells using VFIFE are shown in section "Conclusion".

The VFIFE method

Basic concepts of VFIFE

VFIFE discretizes the structural system into particles, describes the deformation of the structural system by observing the motion of the particles based on Newton's second law, and separates the pure deformation from the rigid body motions by introducing the concept of "reverse rigid body motion". In this part, three basic concepts of VFIFE are demonstrated, including the point description, path unit, and reverse rigid body motion of the element.

Point description. The point description can be regarded as a body composed of spatial particles linked by a set of elements. The motion and configuration of the body are determined by the particles. The elements are deformed following the moving particles, where internal forces arise from. The body configuration depends on the choice of interpolation functions. Therefore, the point description is an approximation of real structure. Shown in Figure 8, the motion and configuration (including the geometry and the spatial position) of a piece of cable can be described by discrete particles (*a, b, c, d*, and *e*), and each two adjacent particles are connected by one cable-link element.

Path unit. To simplify the motion process of the particles, VFIFE disperses the continuous and complicated motion trajectory of particles into several simple motion processes, each of which is called one path unit. Shown in Figure 9, taking particle *c* in Figure 8 as an example, it has a motion path moving from the initial state c_1 to the finial state c_n and disperses the whole time into finite time instants $t_1, t_2 \ldots t_n$. During this process, the motion process between each two time instants can be seen as a path unit as required. It should be noted that the motion of the particle is continuous in one path unit and obeys the governing equations which are based on Newton's second law.

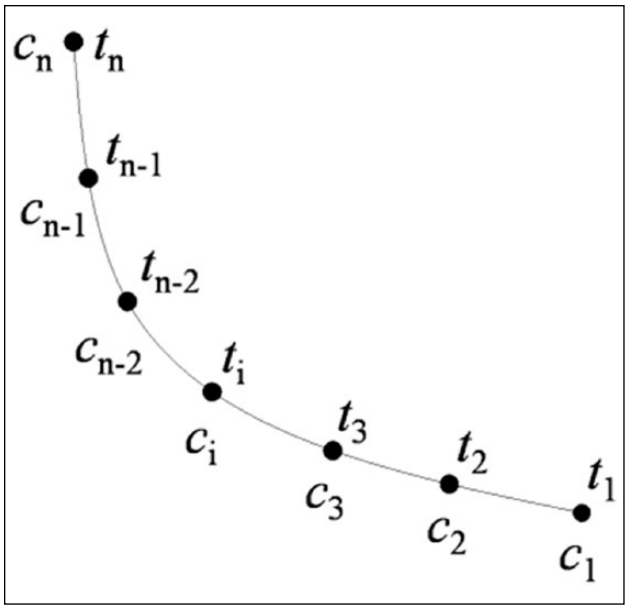

Figure 9. Schematic diagram of the path unit.

Reverse rigid body motion of the element. There is a complicated coupling relationship between the rigid body motion and the pure deformation of the element, and how to get the pure deformation is always the core of the calculation of internal forces. VFIFE estimates the rigid body motion which satisfies the required precision and obtains the pure deformation of the element by deducting the rigid body motion from the whole displacement with the concept of "reverse rigid body motion". Shown in Figure 10, taking element *ab* in Figure 8 as an example, the pure deformation of it in time t_i can be obtained in the following steps. First, translate and rotate the element a_ib_i reversely to $a_{i-1}b_{i2}$ in time t_{i-1} and then obtain the value of the pure deformation of the element easily.

Basic procedure of VFIFE

With the above three concepts, VFIFE is different from the conventional finite element method which is based on continuum mechanics and variational principles. VFIFE models the structural system to be composed of finite particles, and Newton's second law is applied to describe each particle's motion. Therefore, the calculation of VFIFE evolves into a process of solving a set of uncoupled vector form

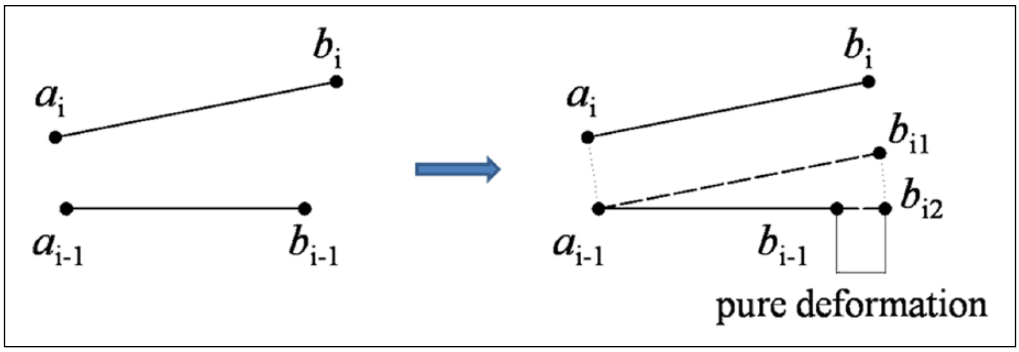

Figure 10. Schematic diagram of the pure deformation.

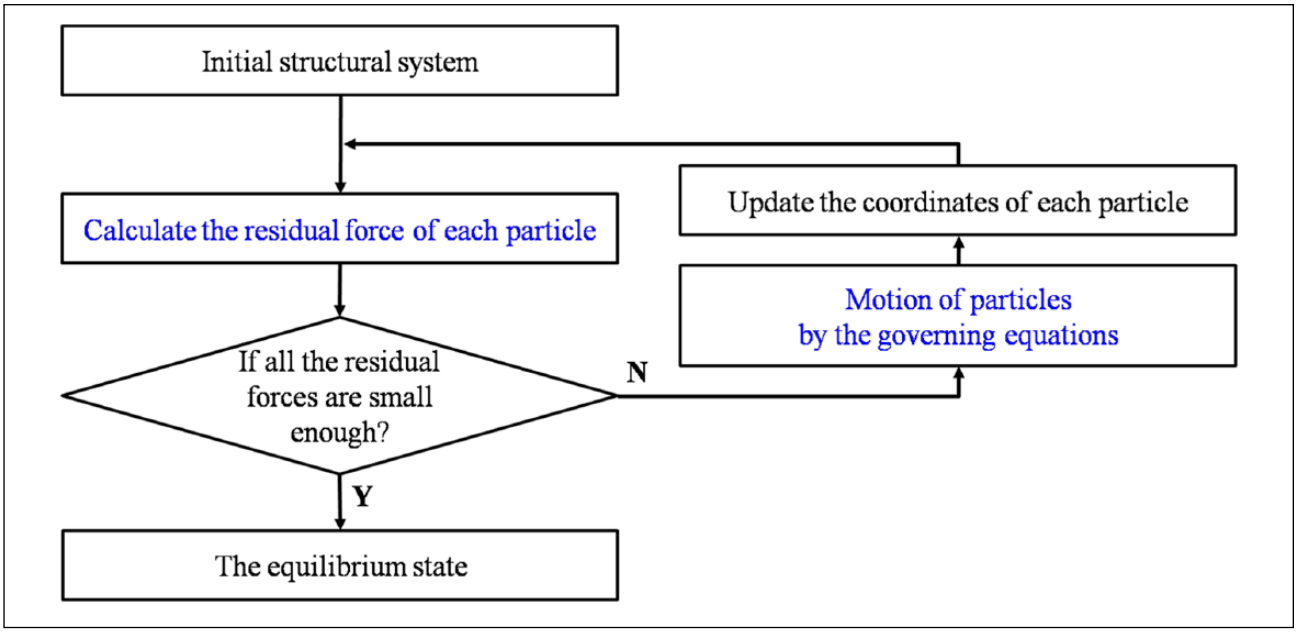

Figure 11. Flowchart of VFIFE.

equations, and the calculation procedure of this method is a step-by-step and particle-by-particle circular computation.

Figure 11 shows the flowchart of VFIFE. It can be described by the following steps:

1. The initial structural system is modeled with a set of particles, and each two adjacent particles are linked with one cable-link element.
2. The residual force of each particle, which is the sum of all the forces acting on a particle from the elements connected to it and the applied loads, is calculated.
3. The largest residual force of all the particles is checked whether it is smaller than the given tolerance which will determine the precision of the calculation. If so, it can be assumed that the equilibrium state of the structural system is generated. Otherwise, continue with the steps below.
4. Analyze the motion of particles by the governing equations based on the Newton's second law, and the displacement of each particle can be obtained.
5. Update the coordinates of each particle and return to step 2 initiating a new calculation looping. Continue the looping until the required precision is achieved.

In the above flowchart, each looping can be seen as one path unit. In each path unit, the motion of each particle is continuous and obeys the governing equations based on Newton's second law. Moreover, two key steps are illustrated here, including the calculation of residual force of each particle and the governing equations of VFIFE.

Calculation of the residual force of each particle. The residual force of each particle is the sum of all the forces acting on a particle from the elements connected to it and the applied

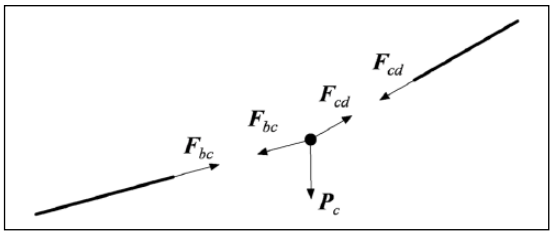

Figure 12. Residual force of particle *c*.

loads. The internal force of the element obeys Hooke's Law in the iteration process introducing the concept of reverse rigid body motion to determine the pure deformation of the element. Taking element *ab* in Figure 10 as an example, the internal force increment of the element ΔF_n in step n can be calculated by equation (1)

$$\Delta F_n = \frac{EAd_{pure}}{l_{n-1}} \tag{1}$$

where EA represents the tensile stiffness of the element, d_{pure} represents the pure deformation of the element in step n, and l_{n-1} represents the length of the element in step $n-1$.

After obtaining the force increment, the internal force of element *ab* in step n can be calculated by equation (2)

$$F_n = \Delta F_n + F_{n-1} \tag{2}$$

where F_{n-1} is the internal force in step $n-1$.

After collecting the internal forces of all the elements, the residual force of each particle can be calculated by the vectorial sum of all the forces acting on the particle. Shown in Figure 12, taking particle *c* in Figure 8 as an example, the residual force $\boldsymbol{F_c}$ in step n can be calculated by equation (3)

$$\boldsymbol{F_c} = \boldsymbol{F_{bc}} + \boldsymbol{F_{cd}} + \boldsymbol{P_c} \tag{3}$$

where $\boldsymbol{F_{bc}}$ and $\boldsymbol{F_{cd}}$ represent the internal forces of elements ***bc*** and ***cd***, and $\boldsymbol{P_c}$ represents the applied loading on particle ***c***.

The governing equations of VFIFE. The governing equations of VFIFE are based on a central difference expression of the Newton's second law. In order to introduce the governing equations clearly, taking the motion of one particle in the $\boldsymbol{x}$ direction as example, the iteration equations of the displacement of the particle can be deduced by the following steps.

According to Newton's second law, there exists the following equation

$$\boldsymbol{F}_n = m\boldsymbol{a}_n \tag{4}$$

The acceleration of the particle can be described using a central difference expression

$$\boldsymbol{a_n} = \frac{\boldsymbol{v}_{n+1/2} - \boldsymbol{v}_{n-1/2}}{h} \tag{5}$$

and the velocities of the particle with a central difference expression

$$\boldsymbol{v}_{n+1/2} = \frac{\boldsymbol{x}_{n+1} - \boldsymbol{x}_n}{h} \tag{6}$$

$$\boldsymbol{v}_{n-1/2} = \frac{\boldsymbol{x}_n - \boldsymbol{x}_{n-1}}{h} \tag{7}$$

Plugging equations (6) and (7) into equation (5) and then into equation (4), the iteration equation of the displacement of the particle can be described as follows

$$\boldsymbol{x}_{n+1} = \frac{h^2}{m}\boldsymbol{F}_n + 2\boldsymbol{x}_n - \boldsymbol{x}_{n-1} \tag{8}$$

However, when $n=1$, x_0 that appeared in equation (8) does not exist. While it noticed that

$$\boldsymbol{v}_1 = \frac{1}{2h}\left(\boldsymbol{x}_2 - \boldsymbol{x}_0\right) \tag{9}$$

x_0 can be described in another way. Finally, the iteration equations of VFIFE can be obtained, which is a Störmer–Verlet integration

$$\begin{cases} \boldsymbol{x}_2 = \dfrac{h^2}{2m}\boldsymbol{F}_1 + \boldsymbol{x}_1 + h\boldsymbol{v}_1 & n = 1 \\ \boldsymbol{x}_{n+1} = \dfrac{h^2}{m}\boldsymbol{F}_n + 2\boldsymbol{x}_n - \boldsymbol{x}_{n-1} & n \geqslant 2 \end{cases} \tag{10}$$

When there exists damping in the structural system, and assuming that the damping force is proportional to the velocity and mass of the particle, we know

$$\boldsymbol{F}_n - \xi m\boldsymbol{v}_n = m\boldsymbol{a}_n \tag{11}$$

where ξ is the damping-mass factor of the particle and it satisfies

$$\xi = \frac{C}{m} \tag{12}$$

where C is the traditional structural damping factor in structural dynamics. However, in VFIFE, C need not to be the real damping factor of the structure, and Wang[26] suggests that ξ satisfies

$$\xi \leqslant \frac{C_{cr}}{m} \tag{13}$$

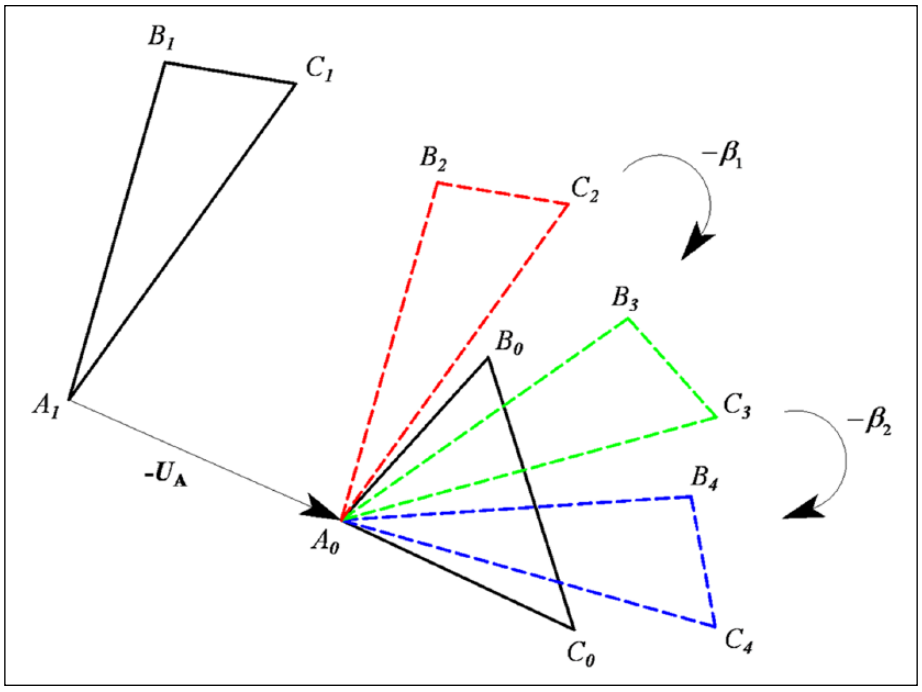

Figure 13. The process of reverse rigid body motion.

where C_{cr} is the critical damping factor of the structure.

With some deduction as above, finally, the iteration equations of VFIFE with viscous damping can be obtained

$$\begin{cases} \boldsymbol{x}_2 = \dfrac{h^2}{2m}\boldsymbol{F}_1 + \boldsymbol{x}_1 + C_2 h \boldsymbol{v}_1 & n = 1 \\ \boldsymbol{x}_{n+1} = \dfrac{C_1 h^2}{m}\boldsymbol{F}_n + 2C_1\boldsymbol{x}_n - C_1 C_2 \boldsymbol{x}_{n-1} & n \geqslant 2 \end{cases} \tag{14}$$

$$C_1 = \frac{1}{1 + 0.5\xi h},\ C_2 = 1 - 0.5\xi h \tag{15}$$

where m represents the mass of the particle, $\boldsymbol{F}$ represents the residual force of $\boldsymbol{x}$ direction acting on it, $\boldsymbol{v}$ represents the velocity of it in the $\boldsymbol{x}$ direction, $\boldsymbol{x}$ represents the coordinate of it in the $\boldsymbol{x}$ direction, n represents the step, and h represents the step length.

It can be observed clearly that equation (14) is an explicit equation, which can get the unknowns from the known quantities. In VFIFE, if the initial coordinates and the initial velocities of the particles are known, it can describe the motion paths of the particles by stepwise derivation using equation (14).

It should be noted that when considering the structural behavior under dead loads, for instance, form-finding problems, two strategies could be applied. One is taking the dead load as a very slowly increased living load (e.g. using an incremental loading method), and the other is adding virtual damping into the equations which aims to eliminate the dynamic effect. Moreover, in order to ensure a better convergence of VFIFE, there are some limits of the step length and the damping-mass factor adopted from-Wang[26], which will not be covered here.

The constant strain triangle element

When considering the form-finding of membrane structures and thus shells, a constant strain triangle element based on VFIFE, which is elastic and isotropic, is developed in this part. According to the framework above, the key point of developing a new element type based on VFIFE is the calculation of the internal force of the element. For the triangular membrane element, two steps are introduced here to calculate its internal force, including the calculation of pure deformation of the element using the concept of reverse rigid body motion and the calculation of internal force increment using its pure deformation.

Calculation of pure deformation of the triangular membrane element. The pure deformation of the triangular membrane element is calculated by introducing the concept of reverse rigid body motion. Shown in Figure 13, taking one triangular membrane element in one path unit as an example, the element ABC moves from $A_0B_0C_0$ to $A_1B_1C_1$ but with an elastic deformation, where A, B, and C represent the names of the three particles. Figure 13 also shows the detailed process that translates and rotates the element reversely from $A_1B_1C_1$ to $A_0B_4C_4$.

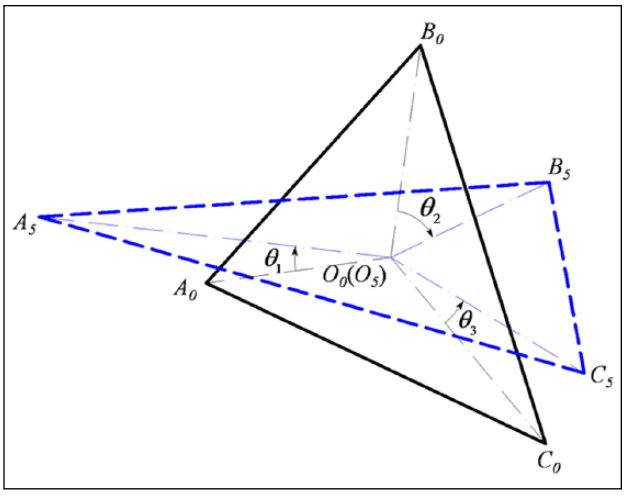

Figure 14. Calculation of β_2.

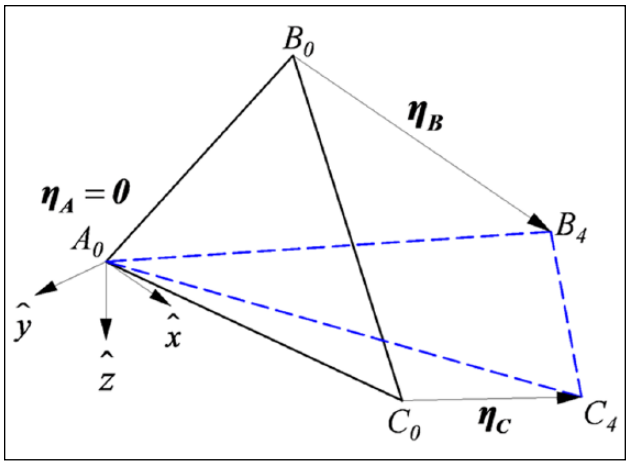

Figure 15. Calculation of the pure deformation.

The pure deformation of this element can be obtained by the following steps.

a. Taking $-\boldsymbol{U}_\mathbf{A}$ as the motion vector, reversely translate the element from $A_1B_1C_1$ to $A_0B_2C_2$, where $\boldsymbol{U}_\mathbf{A}$ is the displacement vector of the particle A in the path unit. Through this process, the rigid body translation is removed from the whole displacement, and as a result, $A_0B_2C_2$ and $A_0B_0C_0$ coincide at point A_0.
b. Taking $-\beta_1$ as the motion angle, reversely rotate the element from $A_2B_2C_2$ to $A_0B_3C_3$, where β_1 is the angle between the normal vectors of $A_1B_1C_1$ and $A_0B_0C_0$. Through this process, the out-of-plane rigid body rotation is removed from the whole displacement, and $A_0B_3C_3$ and $A_0B_0C_0$ are in the same plane.
c. Taking $-\beta_2$ as the motion angle, reversely rotate the element from $A_0B_3C_3$ to $A_0B_4C_4$, where β_2 can be calculated by equation (16)

$$\beta_2 = \frac{\theta_1 + \theta_2 + \theta_3}{3} \tag{16}$$

In order to explain the meaning of $\theta_i\ (i = 1, 2, 3)$, shown in Figure 14, translate $A_0B_4C_4$ to coincide with the centroid of $A_0B_0C_0$ and get $A_5B_5C_5$, where points O_0 and O_5 are the centroids of $A_0B_0C_0$ and $A_5B_5C_5$, respectively, and $\theta_i\ (i = 1, 2, 3)$ represents the angle of relevant midlines of the two triangles. Through this process, the in-plane rigid body rotation is removed from the whole displacement.
d. From the above steps, all the rigid body motions are removed from the whole displacement, $A_4B_4C_4$ is compared with $A_0B_0C_0$, and then the pure deformation of the element can be obtained easily, which can be described by three vectors η_A, η_B, and η_C as shown in Figure 15.

Calculation of the internal force increment of the triangular membrane element. After obtaining the pure deformation of the element, VFIFE calculates the internal force increment by introducing the deformation coordinate system which transforms the space problem to a plane problem. Taking the element and its pure deformation of one path unit in Figure 15 as an example, the deformation coordinate system can be set as follows

$$\hat{\boldsymbol{e}}_1 = \frac{\boldsymbol{\eta}_B}{|\boldsymbol{\eta}_B|} \tag{17}$$

$$\hat{\boldsymbol{e}}_3 = \boldsymbol{n}_0 \tag{18}$$

$$\hat{\boldsymbol{e}}_2 = \hat{\boldsymbol{e}}_3 \times \hat{\boldsymbol{e}}_1 \tag{19}$$

where $\hat{\boldsymbol{e}}_1$, $\hat{\boldsymbol{e}}_2$, and $\hat{\boldsymbol{e}}_3$ represent the unit vectors in the $\hat{x}$, $\hat{y}$, and $\hat{z}$ directions of the deformation coordinate system, respectively, and the vector $\boldsymbol{n}_0$ is the normal vector of $A_0B_0C_0$.

In such deformation coordinate system, where A_0 is the point of origin and the $\hat{x}\hat{y}$ plane is set at the plane of $A_0B_0C_0$ (or $A_0B_4C_4$), the displacement components and thus the force increment components in the $\hat{z}$ direction are zero. Shown in Figure 16, the other displacement components of the displacement vector in this coordinate system are represented as equations (20)–(22), respectively

$$u_A = v_A = 0 \tag{20}$$

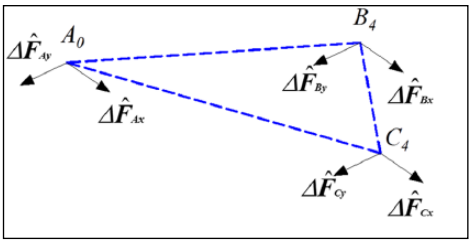

Figure 16. Force increment components and displacement components in the deformation coordinate system.

$$u_B = |\eta_B|, \quad v_B = 0 \tag{21}$$

$$u_C = \eta_C \cdot \hat{e}_1, \quad v_C = \eta_C \cdot \hat{e}_2 \tag{22}$$

where u and v represent the values in $\hat{x}$ and $\hat{y}$ directions, respectively.

After omitting the displacements components which are zero, the displacement vector of the element can be written as

$$\hat{\boldsymbol{u}}_{\cdot} = [u_B \quad u_C \quad v_C]^T \tag{23}$$

So far, the problem of calculation of the internal force increment of the triangular membrane element is quite clear. The displacement vector of the element is known, and the question is to solve the six unknown force increment components of it. In order to solve this problem, the principle of virtual work is applied.

From the virtual work equation, we know (equation (24))

$$\sum_{i=A,B,C} \delta\left(\hat{\boldsymbol{u}}_i\right)^T \Delta\hat{\boldsymbol{F}}_i = \int_V \delta\left(\Delta\hat{\boldsymbol{\varepsilon}}\right)^T \Delta\hat{\boldsymbol{\sigma}} dV \tag{24}$$

where $\hat{\boldsymbol{u}}_i$ and $\hat{\boldsymbol{F}}_i$ represent the displacement vector and the force increment vector of the particle i connected to the element, $\Delta\hat{\boldsymbol{\varepsilon}}$ and $\Delta\hat{\boldsymbol{\sigma}}$ represent the stress increment vector and the strain increment vector of the element, and V represents the volume of the element.

On the contrary, we also understand the relationship of the stress increment and displacement increment of the element, which can be shown as follows (equation (25))

$$\Delta\hat{\boldsymbol{\sigma}} = \boldsymbol{D}\Delta\hat{\boldsymbol{\varepsilon}} = \boldsymbol{D}\boldsymbol{B}^*\hat{\boldsymbol{u}}_{\cdot} \tag{25}$$

where $\boldsymbol{D}$ represents the elastic matrix of the element and isotropic material is just considered in this article, $\boldsymbol{B}^*$ represents the strain–displacement relation matrix of the triangular membrane element, and their concrete expressions are shown in equations (26) and (27), respectively

$$\boldsymbol{D} = \frac{E}{1-\upsilon^2}\begin{bmatrix} 1 & \upsilon & 0 \\ \upsilon & 1 & 0 \\ 0 & 0 & (1-\upsilon)/2 \end{bmatrix} \tag{26}$$

where E represents the elastic modulus of this material, and υ represents Poisson's ratio of it.

$$\boldsymbol{B}^* = \frac{1}{\hat{x}_B\hat{y}_C - \hat{x}_C\hat{y}_B}\begin{bmatrix} \hat{y}_c & -\hat{y}_b & 0 \\ 0 & 0 & \hat{x}_B \\ -\hat{x}_c & \hat{x}_B & -\hat{y}_b \end{bmatrix} \tag{27}$$

where $\hat{x}_B$, $\hat{y}_B$, $\hat{x}_C$, and $\hat{y}_C$ represent the coordinates of point B_0 and C_0 in the deformation coordinate system.

After plugging equation (25) into equation (24) and simplifying it, the force increment vector which includes three force increment components of the element can be calculated by equation (28)

$$\begin{bmatrix} \Delta\hat{F}_{Bx} & \Delta\hat{F}_{Cx} & \Delta\hat{F}_{Cy} \end{bmatrix}^T = d\left(\int_A \boldsymbol{B}^{*T}\boldsymbol{D}\boldsymbol{B}dA\right)\hat{\boldsymbol{u}}_{\cdot} \tag{28}$$

where d and A represent the thickness and area of the triangular element. Three of the six unknown force increment components have been solved so far. For solving the other three force increment components, establish the equilibrium equations of the element shown in equations (29)–(31), which, respectively, represent that the sum of moments in point A_0 and the sum of force component in the $\hat{x}$ and $\hat{y}$ directions are all equal to zero

$$\sum \hat{M}_A = 0 \tag{29}$$

$$\sum \hat{F}_x = 0 \tag{30}$$

$$\sum \hat{F}_y = 0 \tag{31}$$

The other three force increment components can be calculated by the following equations

$$\Delta\hat{F}_{By} = \frac{1}{\hat{x}_B}\left(\Delta\hat{F}_{Bx}\hat{y}_B + \Delta\hat{F}_{Cx}\hat{y}_C - \Delta\hat{F}_{Cy}\hat{x}_C\right) \tag{32}$$

$$\Delta\hat{F}_{Ax} = -\left(\Delta\hat{F}_{Bx} + \Delta\hat{F}_{Cx}\right) \tag{33}$$

$$\Delta\hat{F}_{Ay} = -\left(\Delta\hat{F}_{By} + \Delta\hat{F}_{Cy}\right) \tag{34}$$

However, it should be noted that the force increment components that we obtain now are described in the deformation coordinate system. When they are involved in calculating residual forces of the particles, all the force increment components should first be transformed from

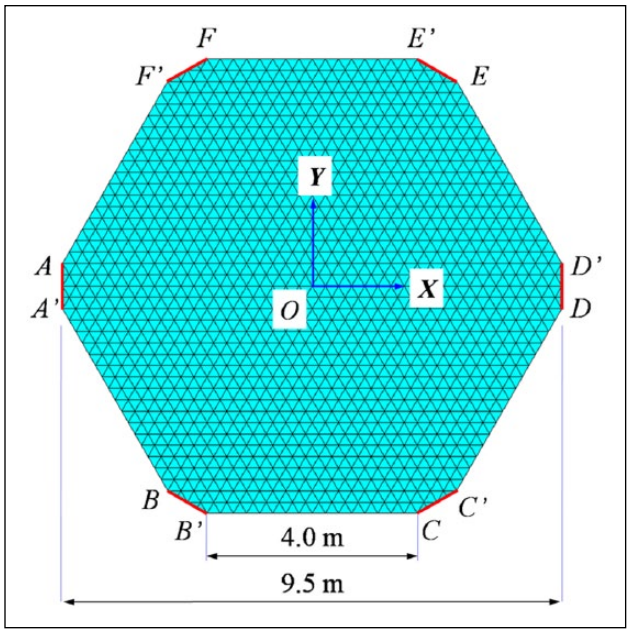

Figure 17. Initial conditions of *Example 1*.

triangle $A_0B_4C_4$ (which is in the deformation coordinate system) to triangle $A_1B_1C_1$ (which is the end position of the path unit), and then to the global system.

In conclusion, the framework of VFIFE based on the cable-link element is explained first, and a constant strain triangle element is introduced subsequently. According to the above works, a common procedure in the platform of MATLAB is programmed in this article.

Numerical form-finding of shell structures

In this section, using VFIFE, form-finding of shells which are generated from hanging models, tension models, and pneumatic models is discussed. One numerical example is presented in each kind of form-finding. Moreover, in order to verify the capability of VFIFE in finding optimal structural shapes for shells, structural analysis of these form-found shells is conducted.

Numerical form-finding of shells generated from hanging models

Hanging models represent a type of equilibrium state of flexible materials under their self-weight and certain constraint conditions with stress states in pure tension. When these equilibrium shapes are used as the geometry of rigid structures after inverting them, they will perform with an effective structural behavior under their self-weight or equally distributed loading.

Figure 17 shows the initial conditions of *Example 1*. The initial shape of this example is a hexagon in the ***XY*** plane with supports at the six corners, and the corners are beveled by lines *AA'*, *BB'*, *CC'*, *DD'*, *EE'*, and *FF'*. The plane area is 64.30 m^2 (hexagon with sides of 5.0 m). The initial numerical structural model is composed of particles and triangular membrane elements. The elastic modulus of the membrane material is 5.0E05 N/m^2, Poisson's ratio is 0.3, and the thickness of the membrane element is 0.001 m. In VFIFE, the mass of the structure is distributed to the particles; in this example, masses of the internal particles are 0.1 kg and those of the boundary particles are 0.05 kg.

With the above initial conditions, it uses VFIFE to carry out form-finding of this membrane structure under its self-weight. In the calculation process, the step length h is set to 5.0E-03, the damping-mass factor ξ is set to 15.0, and the tolerance of the residual force is set to 0.001 N. After the calculation with 2211 steps, it approaches the equilibrium shape of the hanging membrane which meets the tolerance of the residual force in each particle, and Figure 18 shows the inverted shape and its coordinate system. In order to demonstrate the calculation process, Figure 19 shows the evolution curve of the biggest residual force of the particles by steps, in which the straight line represents that the load is using an incremental loading method in this static equilibrium problem.

Then, structural static analysis of this form-found shell under its self-weight is conducted using ANSYS software. The material of this shell is concrete, with an elastic modulus of 2.10E4 MPa, Poisson's Ratio of 0.20, and density of 2500 kg/m^3. The thickness of this shell is 0.04 m. The acceleration of gravity is 9.80 m/s^2. The shell is simply supported at six corners. After analysis, Figures 20–22 present the principal stresses (S1, S2 and S3) at the middle surface of the shell, and Figures 23 and 24 present vectorial representations of the principal stresses. In these contour plots, principal stresses S1, S2, and S3 are positive for the tension stress state and negative for the compression stress state. It can be observed that in the perpendicular directions of the shell principal stress, S1 is very small and tension stresses occur only at a very small part, while in the other two perpendicular principal directions in the plane tangent of the shell, principal stresses S2 and S3 are totally in compression stress states. This means the form-found shell has a good shell behavior.

Numerical form-finding of shells generated from tension models

Tension models are typical "self-stressing" structural systems, with their stiffness resulting from a system of internal stresses in static equilibrium and with their stress conditions also being pure tension. These equilibrium shapes of tension models can also be used for the development of geometries of shells.

Figure 25 shows the initial conditions of *Example 2*, most of which are the same as *Example 1*. However, the

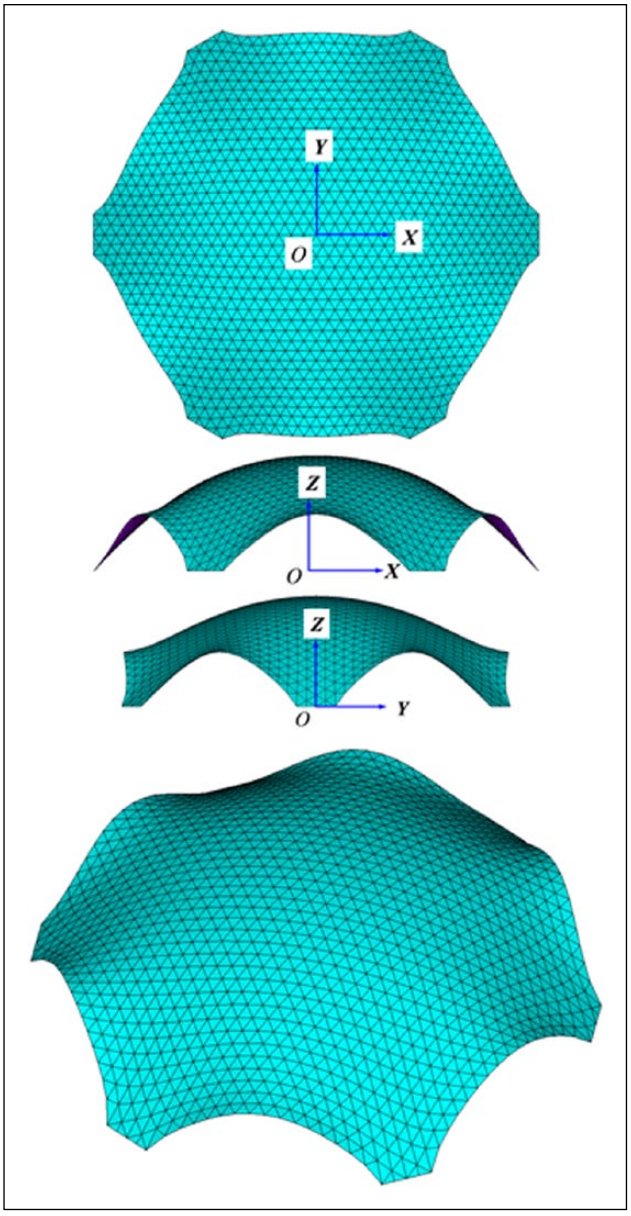

Figure 18. Form-finding result of *Example 1*.

gravity of each particle is not considered in this example. The membrane elements of this structural model have a pre-stress of 10.0 kPa. In the center of the initial shape, the particles in the boundary lines of the hexagon *GHIJKL* with sides of 0.75 m will be uplifted 5.0 m. Moreover, cable elements are applied in the boundary lines *A′B, B′C, C′D, D′E, E′F* and *F′A*, the elastic modulus of the cable is 1.0E06 N/m^2, the cross-sectional area of it is 0.01 m^2, and the pre-stress of it is 50.0 kPa.

In the calculation process of VFIFE, except that the damping-mass factor ξ is set to 10.0, other parameters match with *Example 1*. After the calculation with 3336 steps, it approaches the equilibrium shape of a tent structure, as shown in Figure 26. Figure 27 shows the evolution

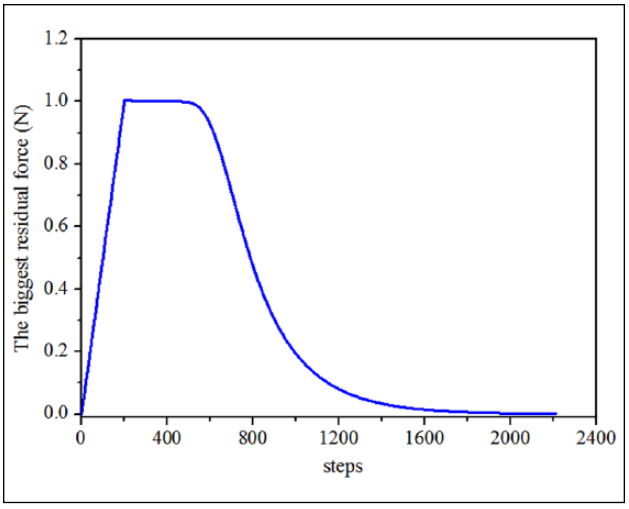

Figure 19. The evolution curve of VFIFE of *Example 1*.

curve of the maximum value of residual force of the particles by steps.

Then, structural static analysis of this form-found shell under vertically downward load is conducted. The material and geometric parameters correlate with *Example 1*. In this analysis, the shell is simply supported at six corners, the load of 1.00 kN acts on the hexagon *GHIJKL*, and their lateral displacements are constrained; moreover, the self-weight of this shell is not considered. After analysis, Figures 28–32 present the same results as *Example 1*. It can be seen that the principal stresses S1, S2 and S3 are totally in compression stress states, which means this form-found shell has a good shell behavior.

Numerical form-finding of shells generated from pneumatic models

Pneumatic models represent a type of equilibrium state of flexible materials under air pressure and certain constraint conditions, where stress states are in pure tension. These equilibrium shapes of pneumatic models can be used as the geometry of shells and can also be adopted as molds in the construction process.

Figure 33 shows the initial conditions of *Example 3*, and the overall conditions are the same as *Example 1*. However, all the boundary lines are constrained in this example. There is no pre-stress in the membrane elements. The air pressure applied to this membrane is 25.0 kPa. Similar to *Example 2*, the gravity of each particle is not considered in this example.

In the calculation process of VFIFE, all the parameters are the same as *Example 2*. After the iteration calculation (which includes 7559 steps), it finally approaches the equilibrium shape of the pneumatic membrane structure, which is shown in Figure 34. Figure 35 shows the curve of evolution of the highest value of residual force of the particles by

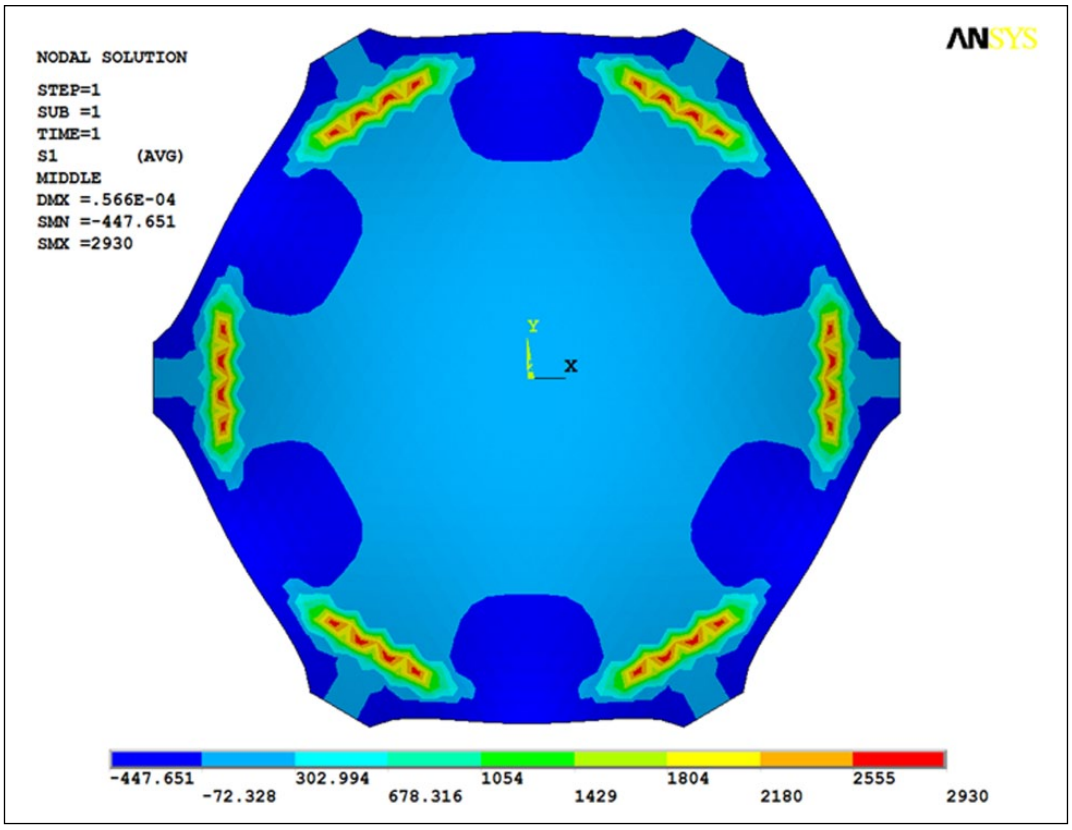

Figure 20. Principal stress S1 at the middle surface of the shell of *Example 1* (Pa).

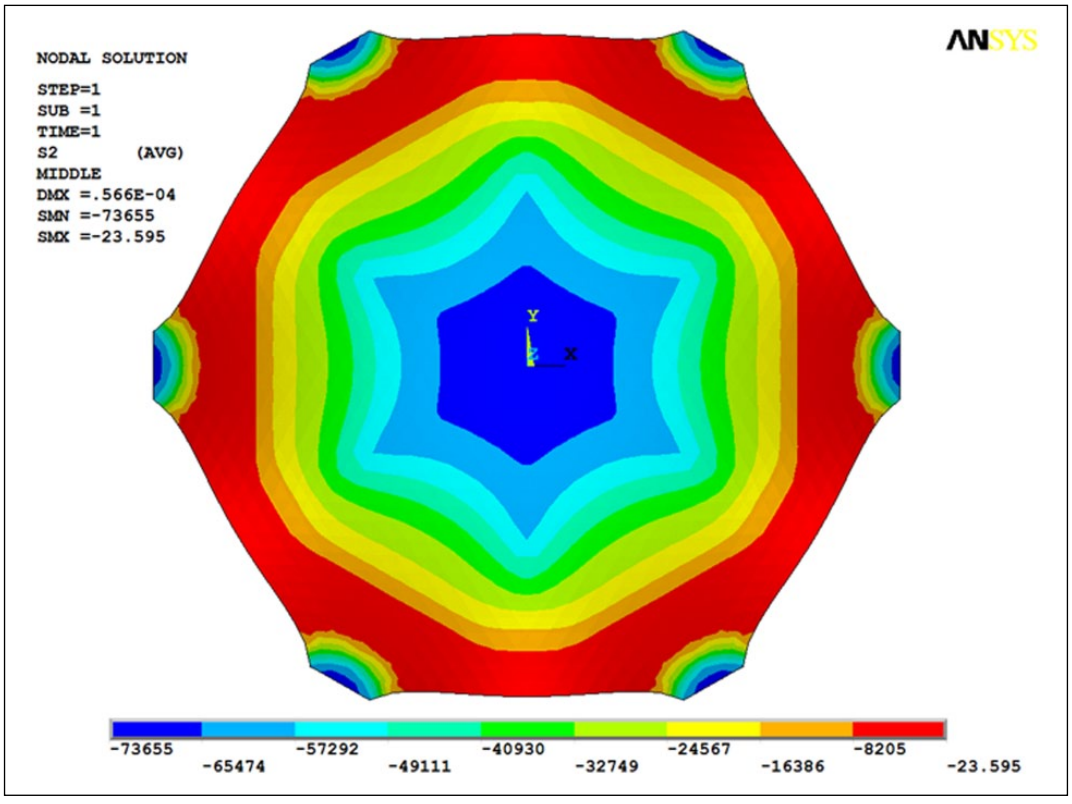

Figure 21. Principal stress S2 at the middle surface of the shell of *Example 1* (Pa).

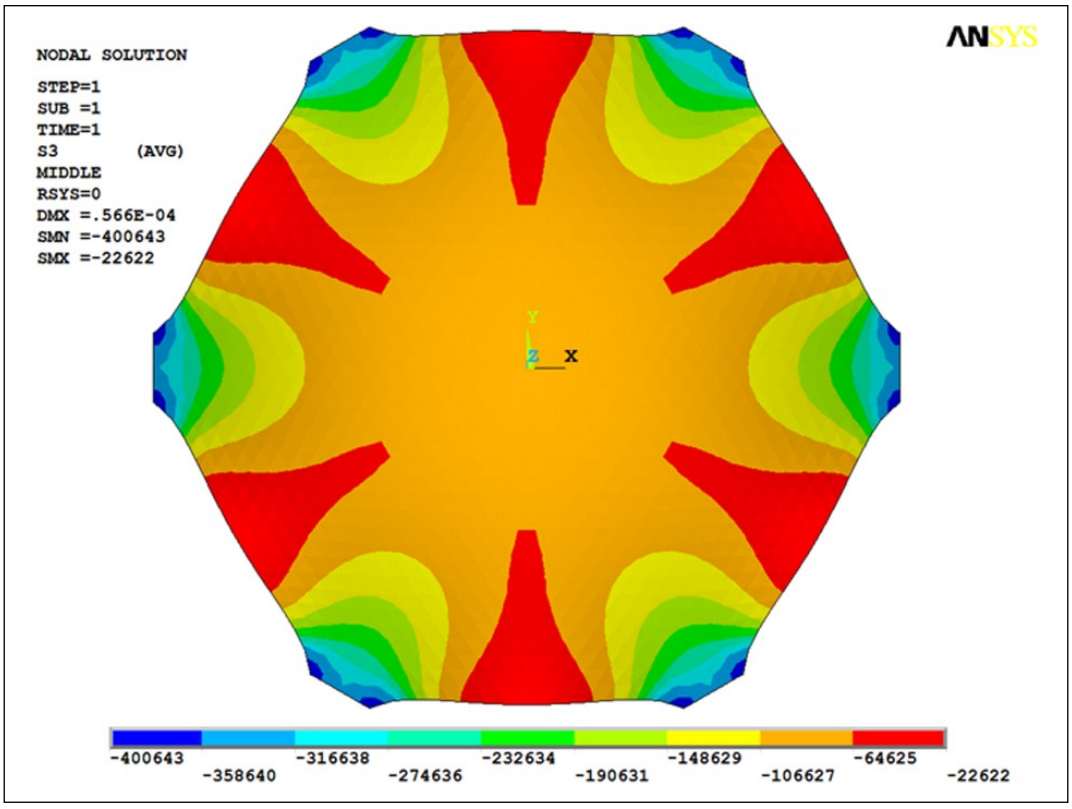

Figure 22. Principal stress S3 at the middle surface of the shell of *Example 1* (Pa).

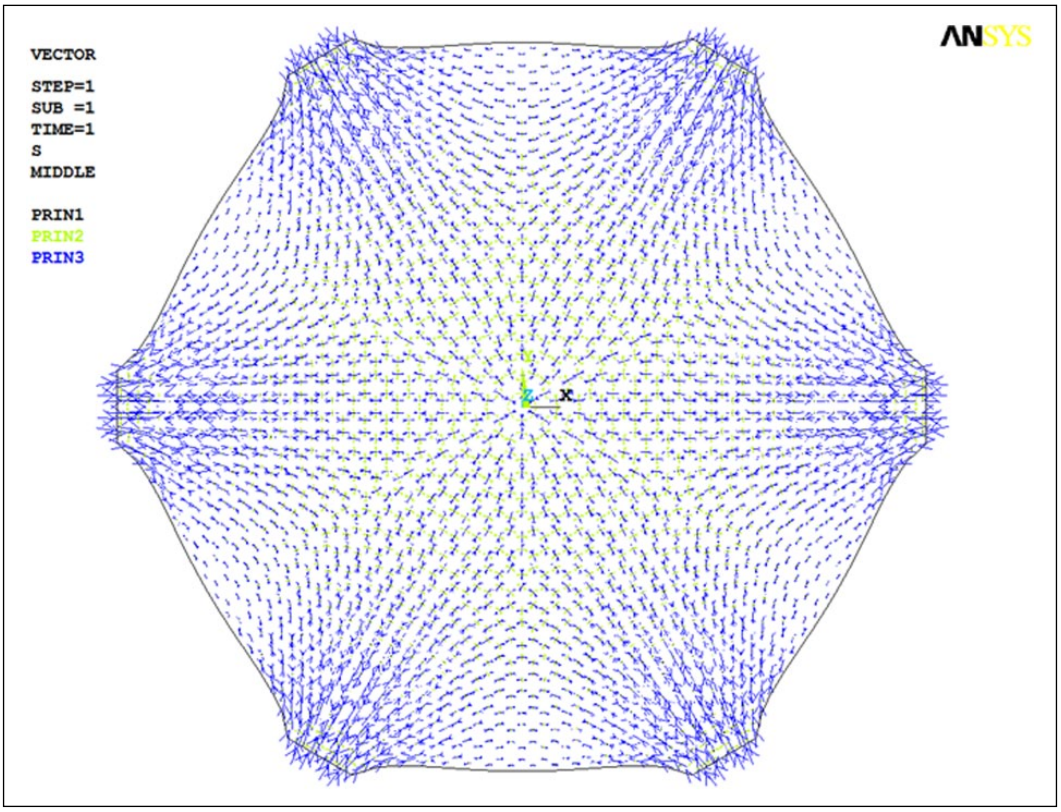

Figure 23. Vectorial representation of the principal stresses of the shell of *Example 1*.

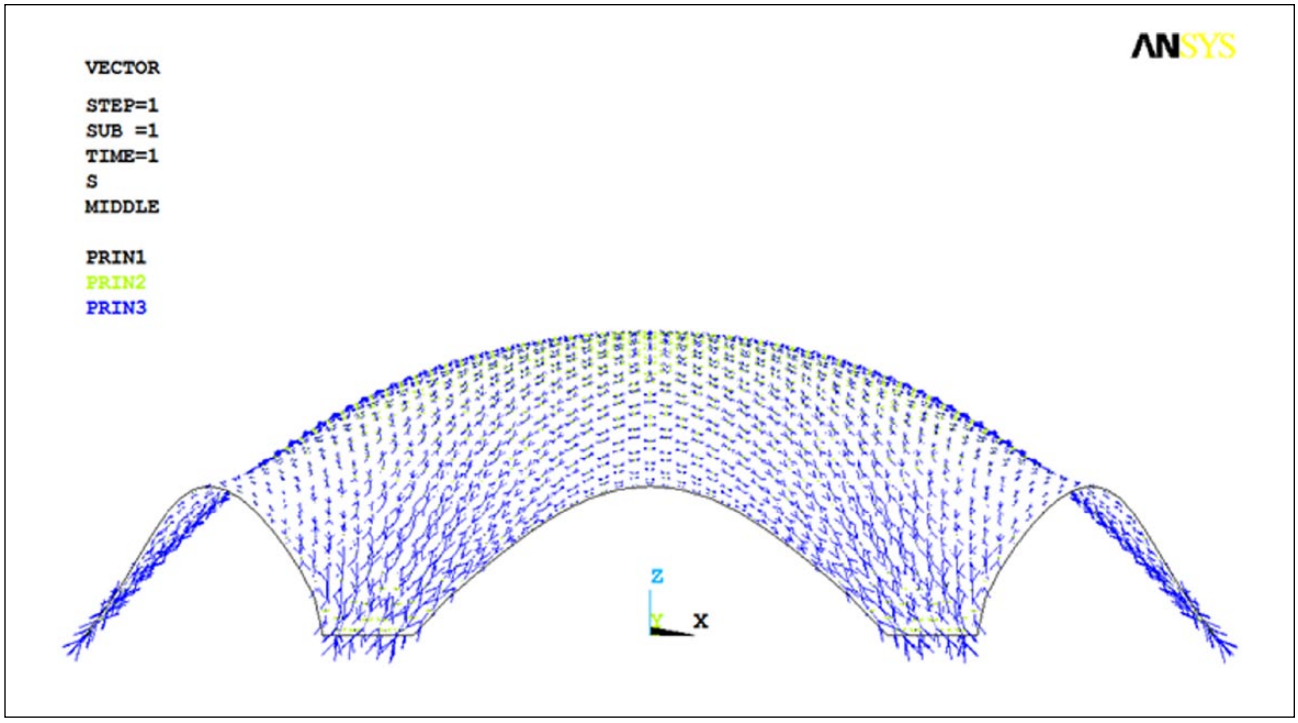

Figure 24. Vectorial representation of the principal stresses of the shell of *Example 1* (lateral view).

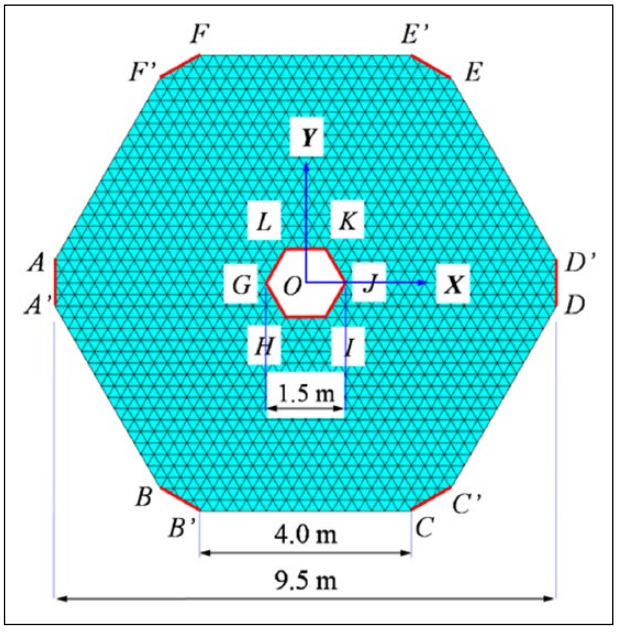

Figure 25. Initial conditions of *Example 2*.

steps, in which the straight line represents that the air pressure is applied by an incremental loading method.

Then, structural static analysis of this form-found shell under its self-weight is conducted. The material and geometric parameters are the same as *Example 1*. The shell is simply supported along the edges. After analysis, Figures 36–40 present similar results as *Example 1*. It can be seen that the principal stresses S1, S2 and S3 are totally in compression stress states, which means the form-found shell has a good shell behavior.

Characteristics of VFIFE in form-finding problems

From the above three form-finding examples that use fictitious properties, it can be observed that VFIFE is feasible and accurate enough in all the three types of form-finding problems. And in this part, two main characteristics are introduced as follows:

1. In VEIFE, there is no need to establish the stiffness matrix in the calculation process, which overcomes problems such as stiffness matrix singularity and iterative convergence difficulty in the traditional finite element method. For form-finding problems, VFIFE can generate the equilibrium structural form from any unbalanced state with arbitrary and inaccurate specification of geometry, which brings great convenience for solving these kinds of problems with strong nonlinearity.

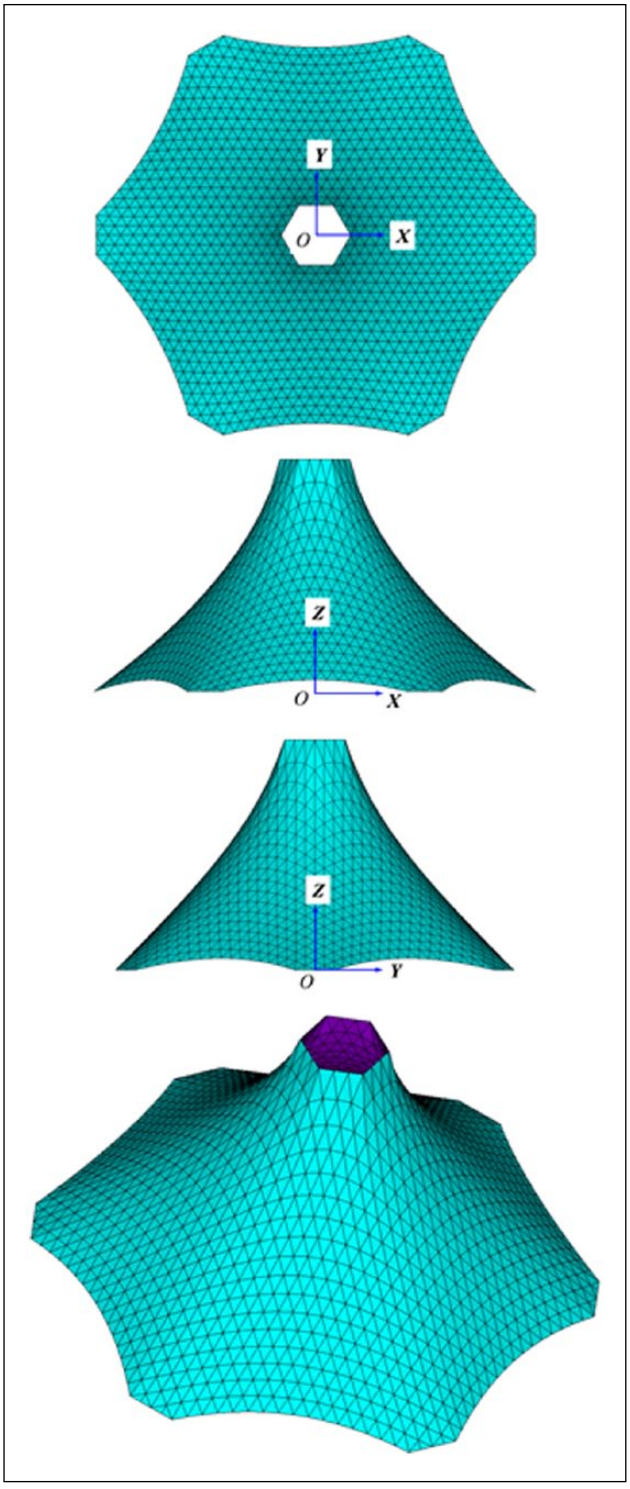

Figure 26. Form-finding result of *Example 2*.

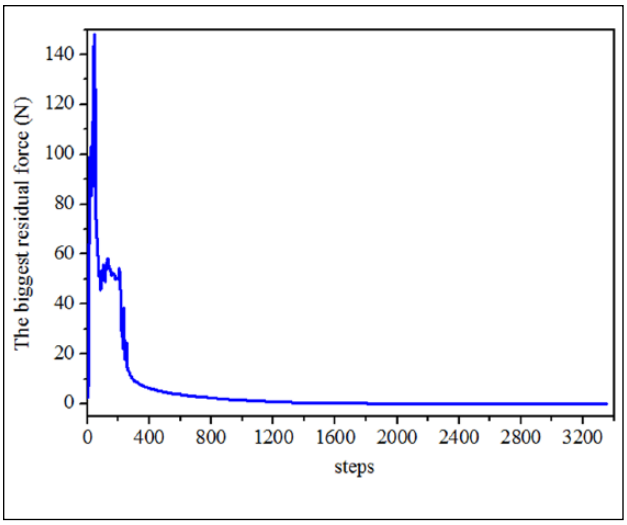

Figure 27. The evolution curve of VFIFE of *Example 2*.

2. According to its governing equations, VFIFE observes the structural behavior by describing the motion of the particles. Therefore, it can reflect the real physical motion process of the structures. For some analysis problems including complex structural behavior, the complete deformation process might need to be observed. For instance, the inflation process of the pneumatic model of *Example 3* can be obtained, and Figure 41 shows some intermediate states during the whole calculation process.

Conclusion

This article introduces VFIFE to carry out form-finding of shells which are generated from physical models, and in order to demonstrate the capability of VFIFE in finding optimal structural shapes for shells, structural static analyses of these form-found shells are conducted. The main works are the following:

1. Form-finding of shells generated from three kinds of physical models, which are hanging models, tension models and pneumatic models, is concluded in this article. Several typical projects generated from physical models and some numerical means for form-finding of shells are introduced.
2. Taking the cable-link element as example, the framework of VFIFE is explained with three basic concepts, including the point description, the path unit, and the reverse rigid body motion of the element. According to this, a constant strain triangle element is introduced, and relevant required equations are deduced.
3. By simulating the equilibrium shapes of physical models using VFIFE, form-finding of shells is discussed in this article with three numerical

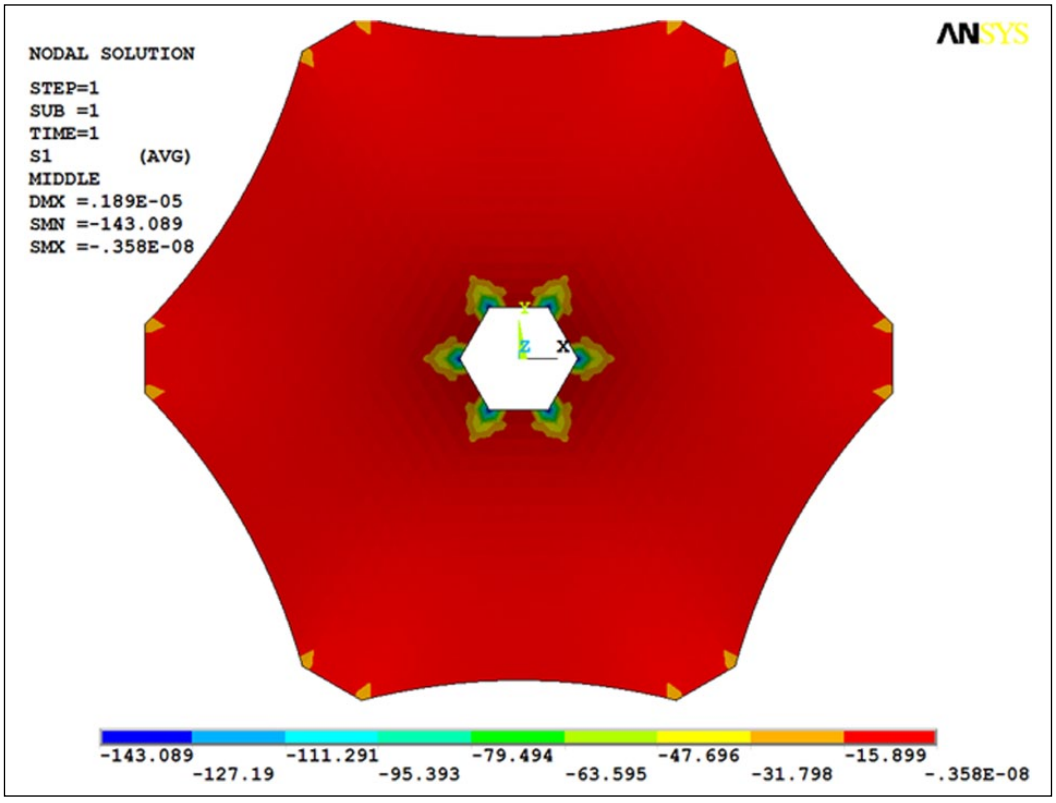

Figure 28. Principal stress S1 at the middle surface of the shell of *Example 2* (Pa).

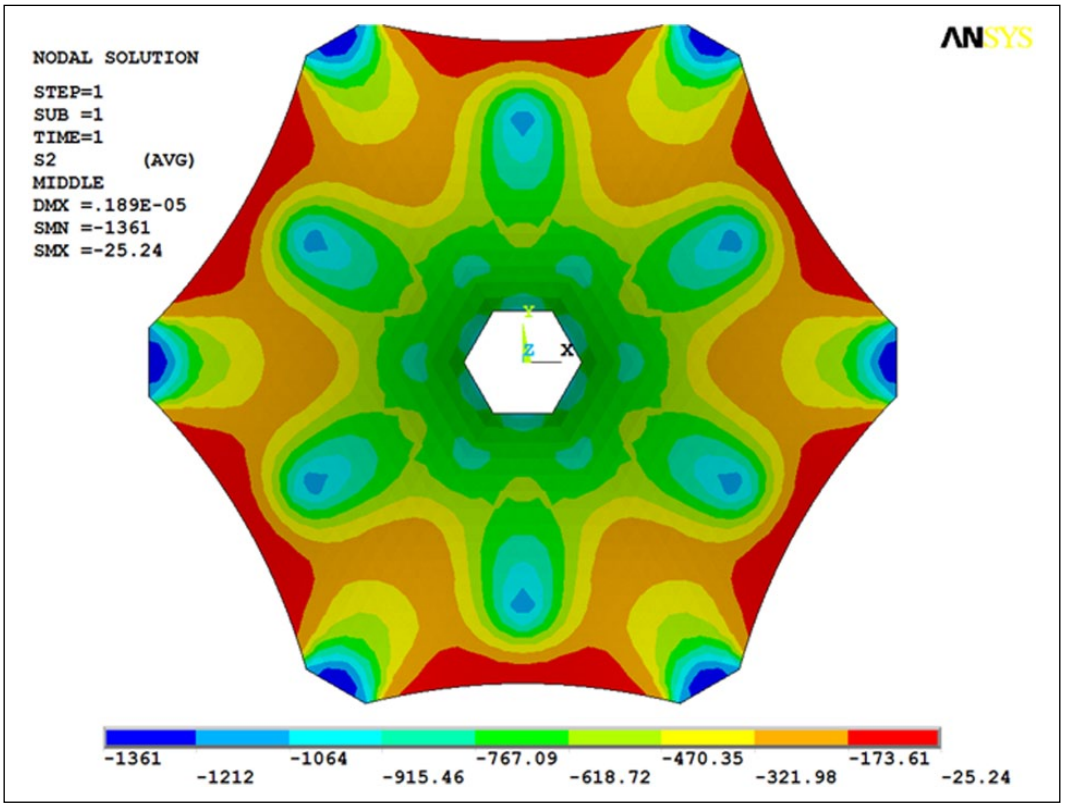

Figure 29. Principal stress S2 at the middle surface of the shell of *Example 2* (Pa).

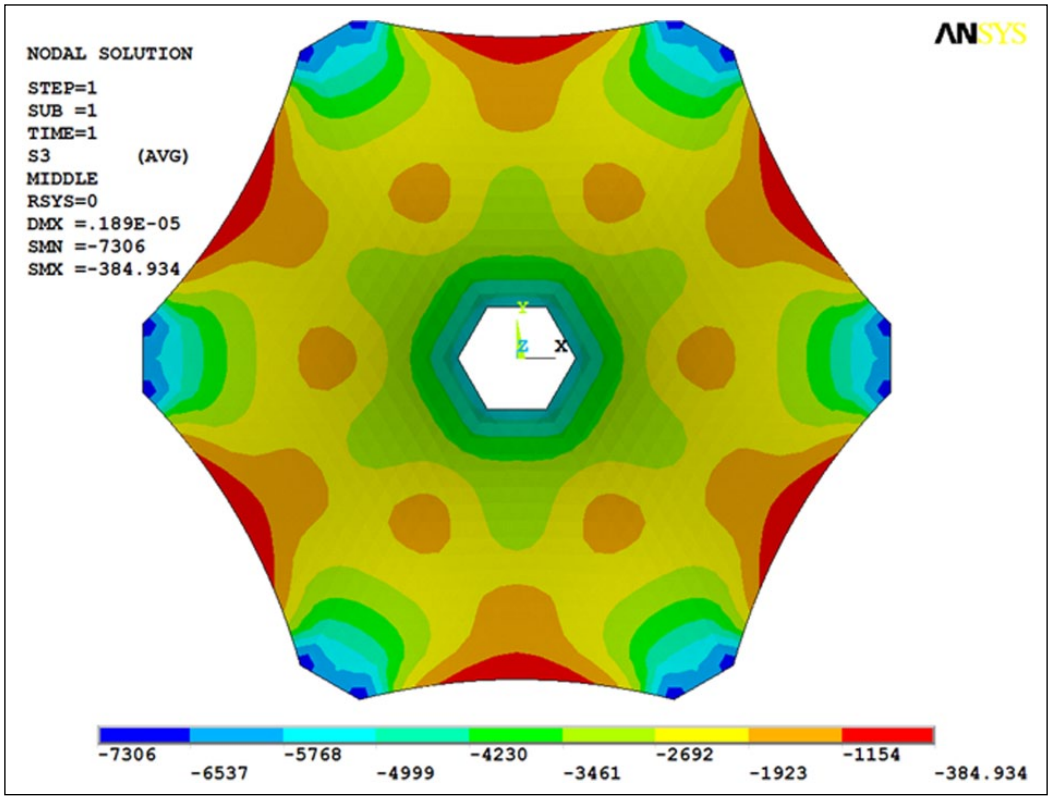

Figure 30. Principal stress S3 at the middle surface of the shell of *Example 2* (Pa).

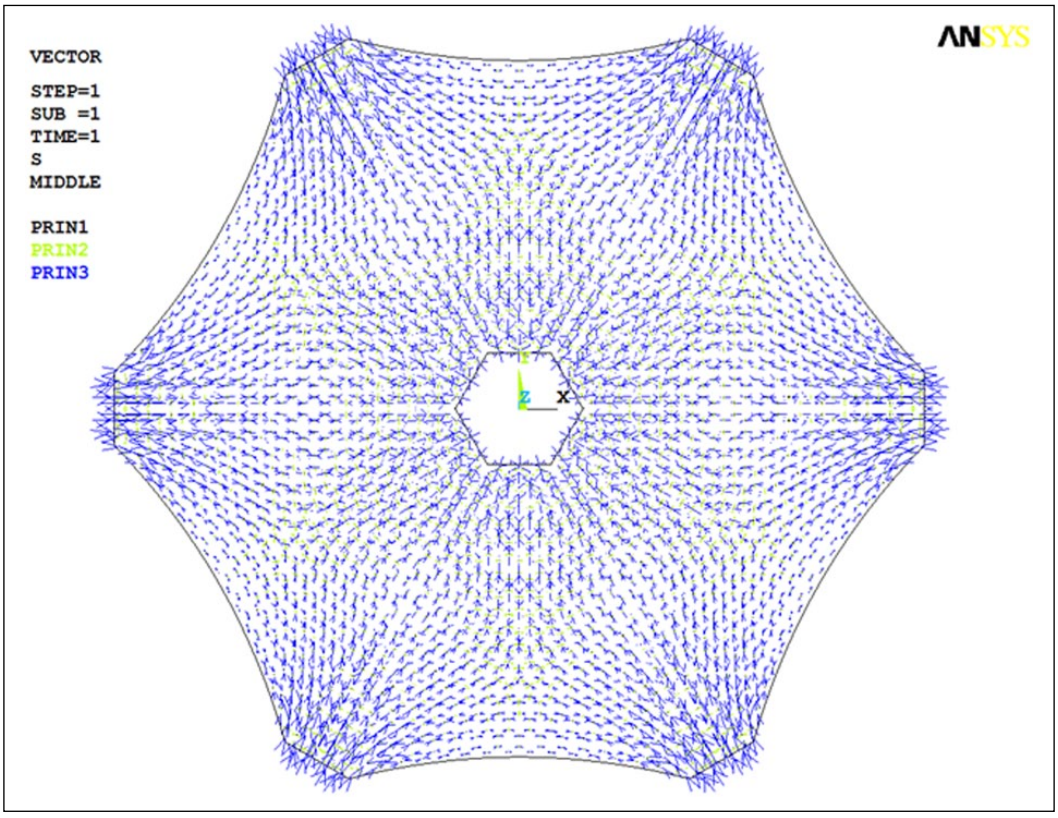

Figure 31. Vectorial representation of the principal stresses of the shell of *Example 2*.

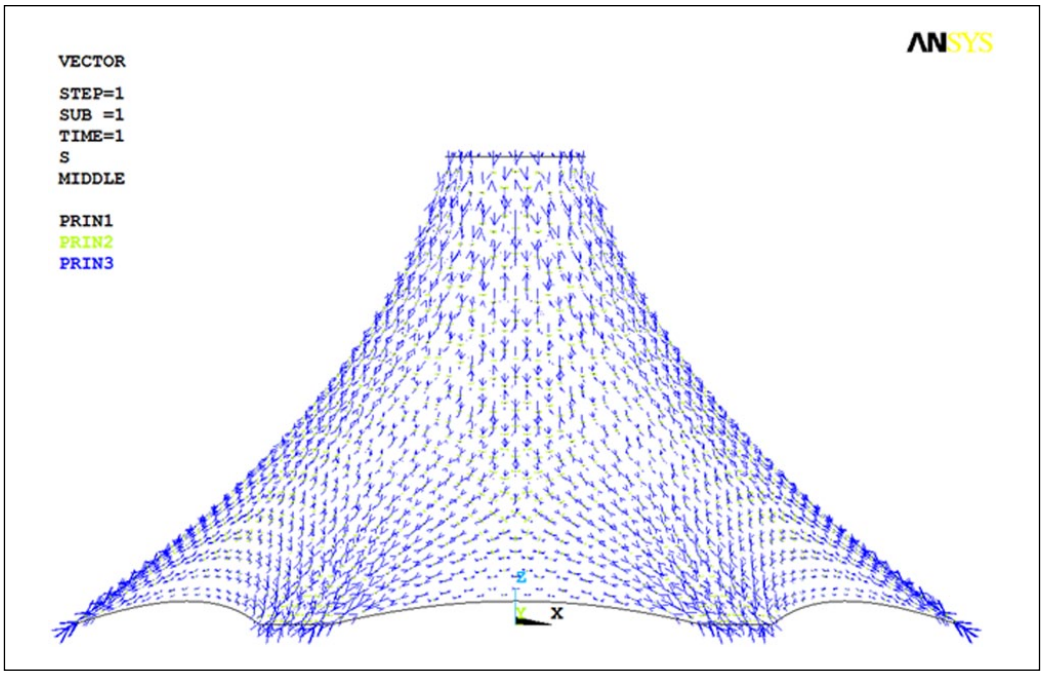

Figure 32. Vectorial representation of the principal stresses of the shell of *Example 2* (lateral view).

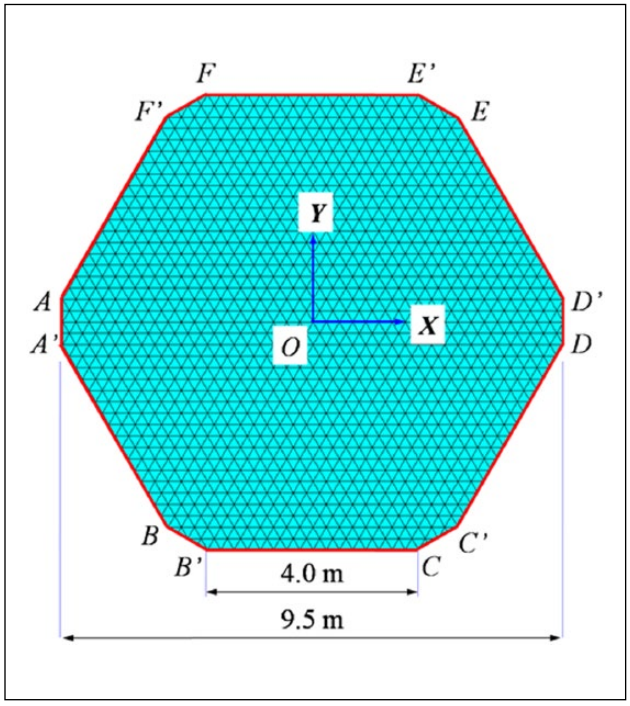

Figure 33. Initial conditions of *Example 3*.

examples. After structural analysis of these form-found shells, the capability of VFIFE in finding optimal structural shapes for shells is verified.

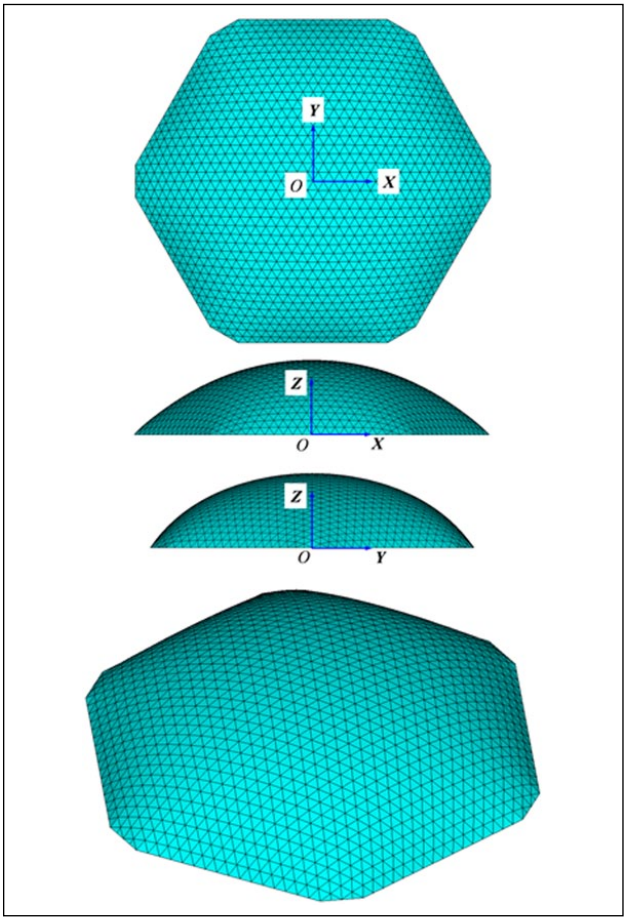

Figure 34. Form-finding result of *Example 3*.

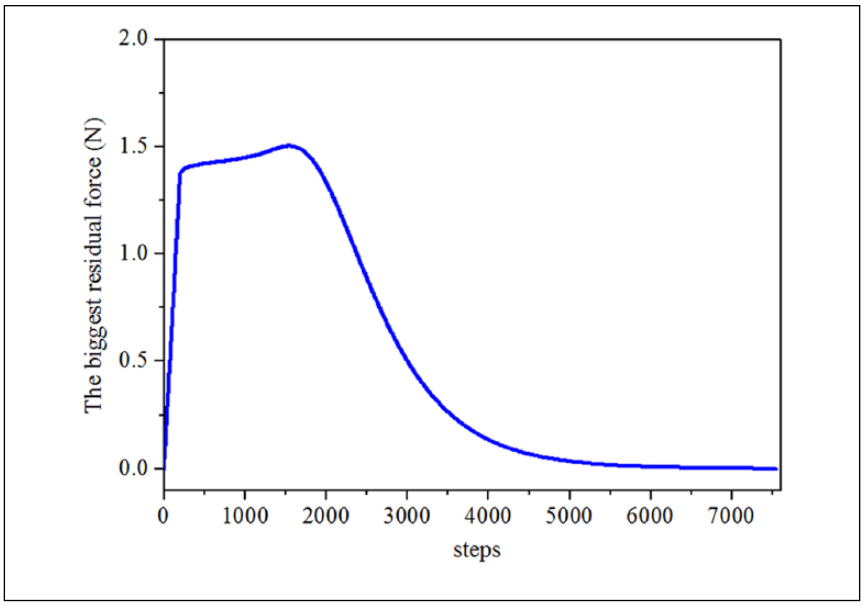

Figure 35. The evolution curve of VFIFE of *Example 3*.

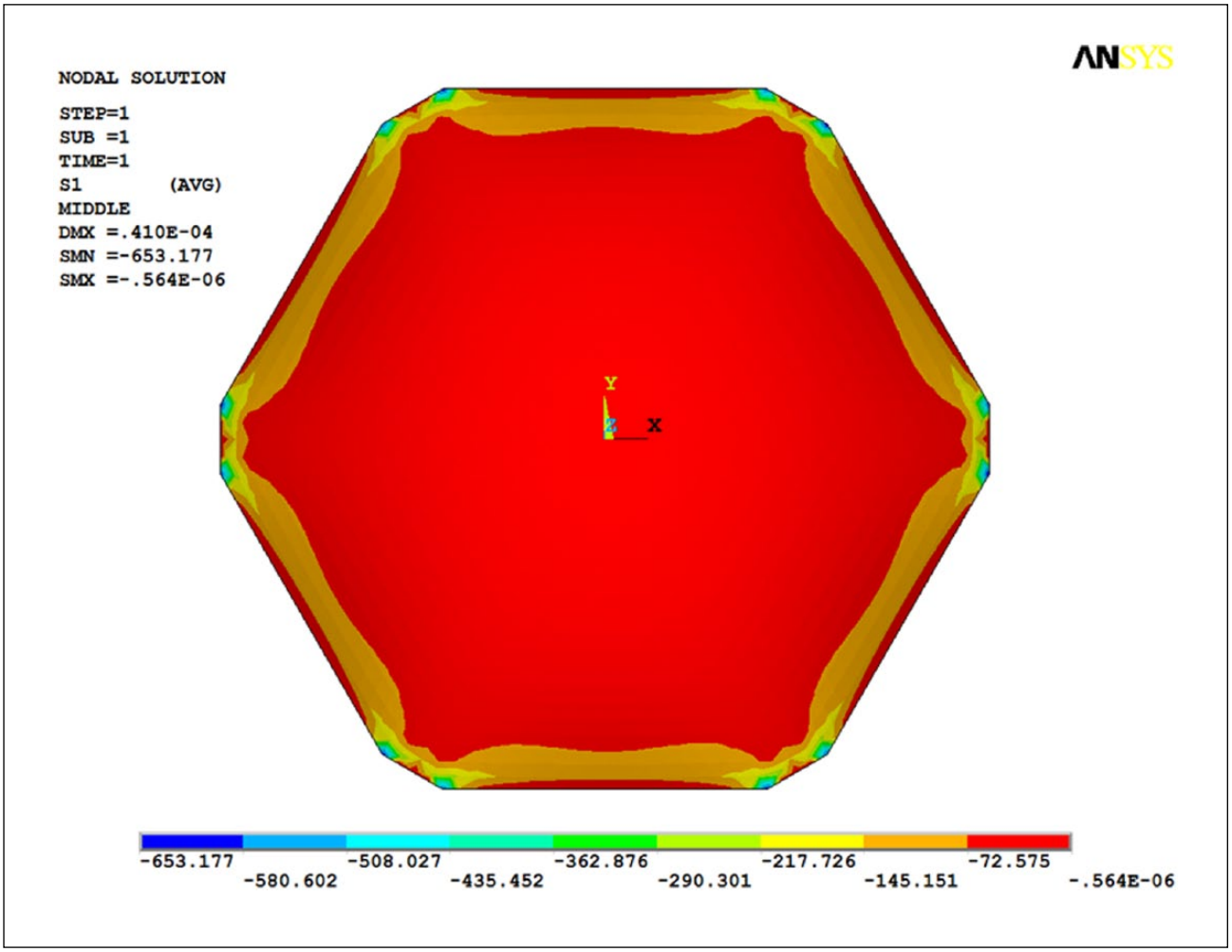

Figure 36. Principal stress S1 at the middle surface of the shell of *Example 3* (Pa).

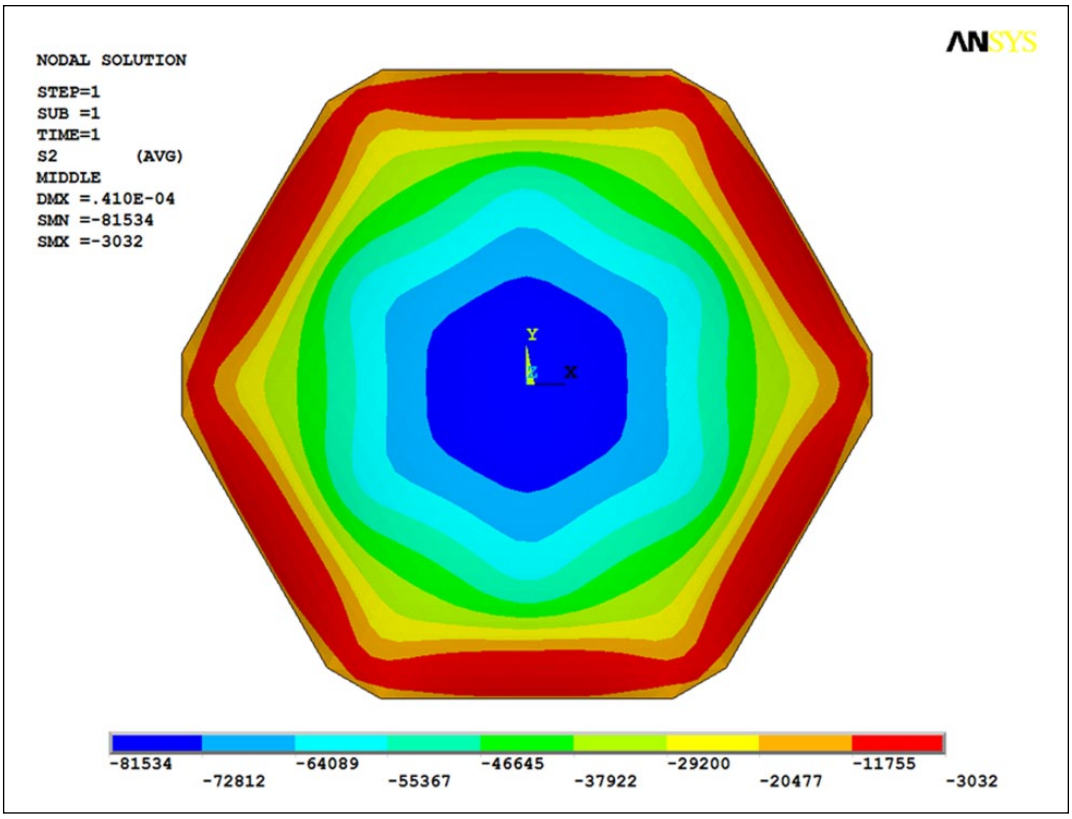

Figure 37. Principal stress S2 at the middle surface of the shell of *Example 3* (Pa).

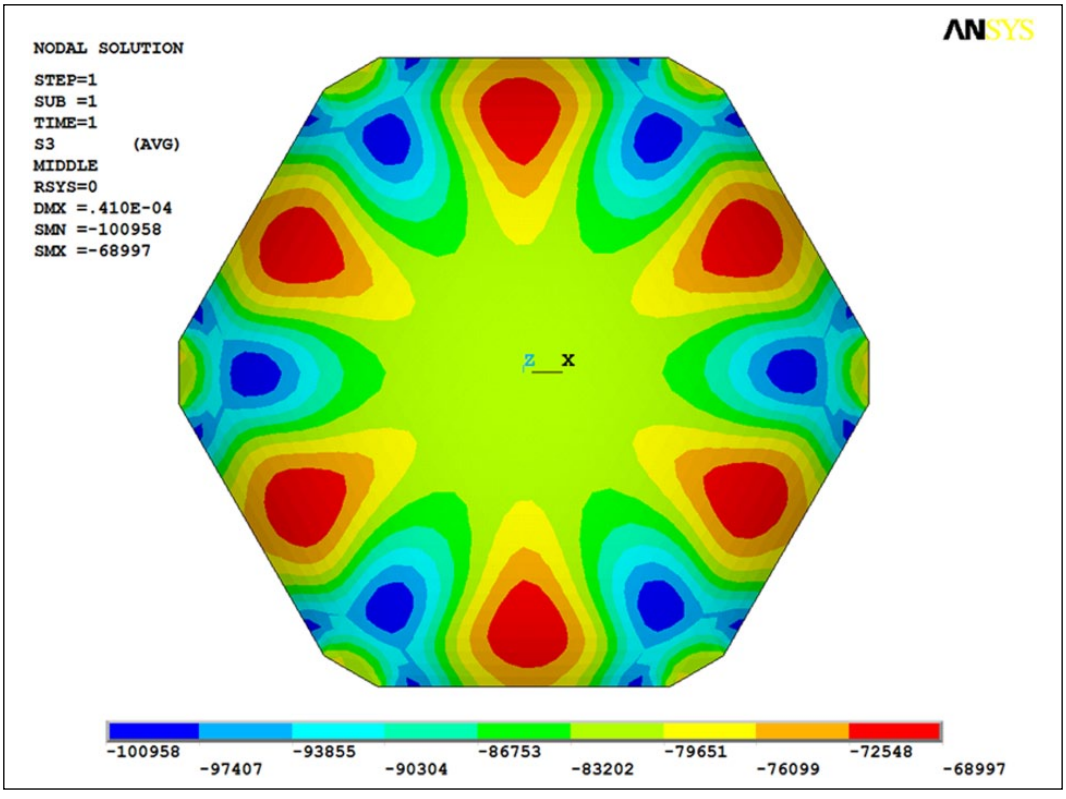

Figure 38. Principal stress S3 at the middle surface of the shell of *Example 3* (Pa).

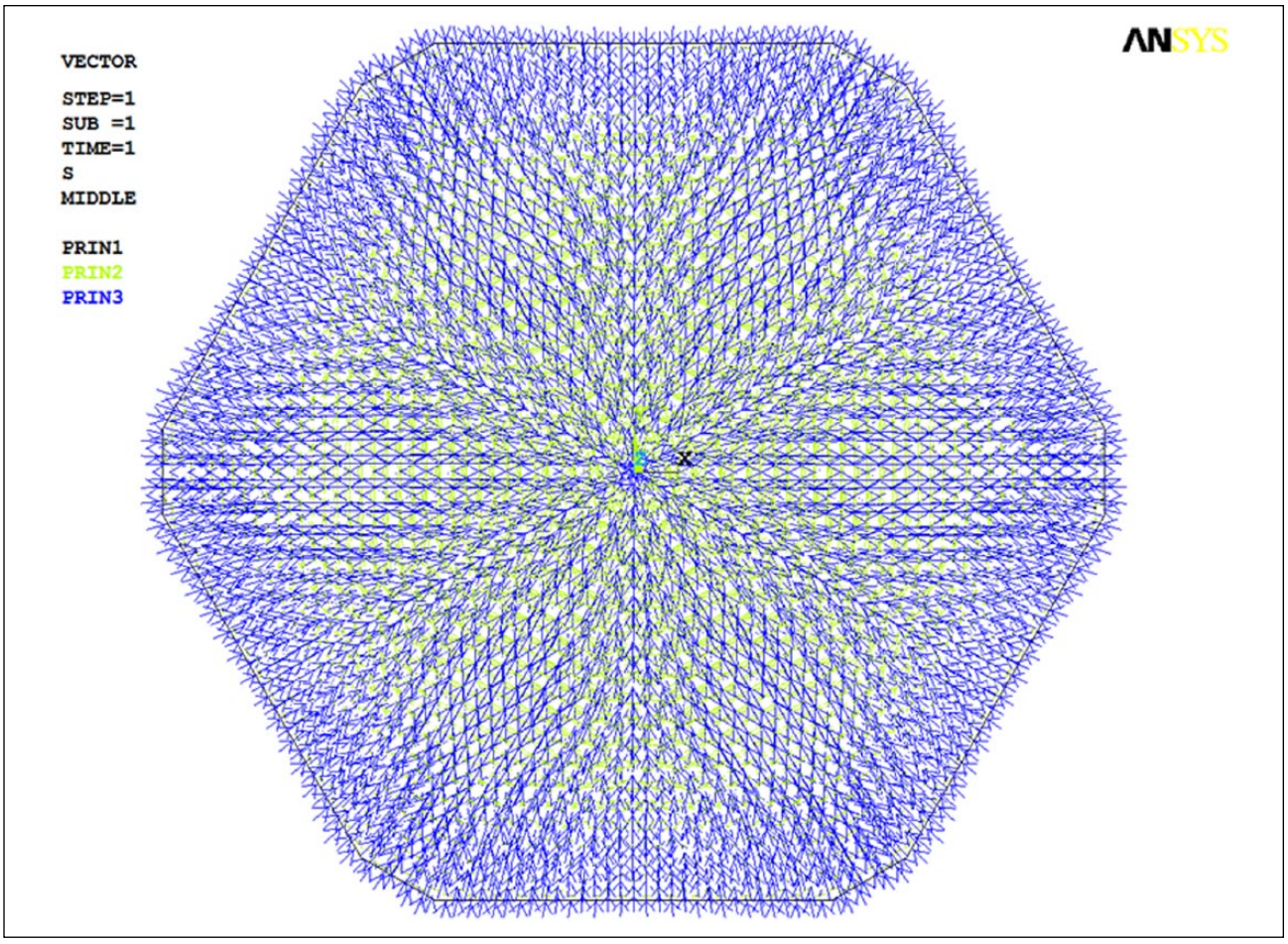

Figure 39. Vectorial representation of the principal stresses of the shell of *Example 3*.

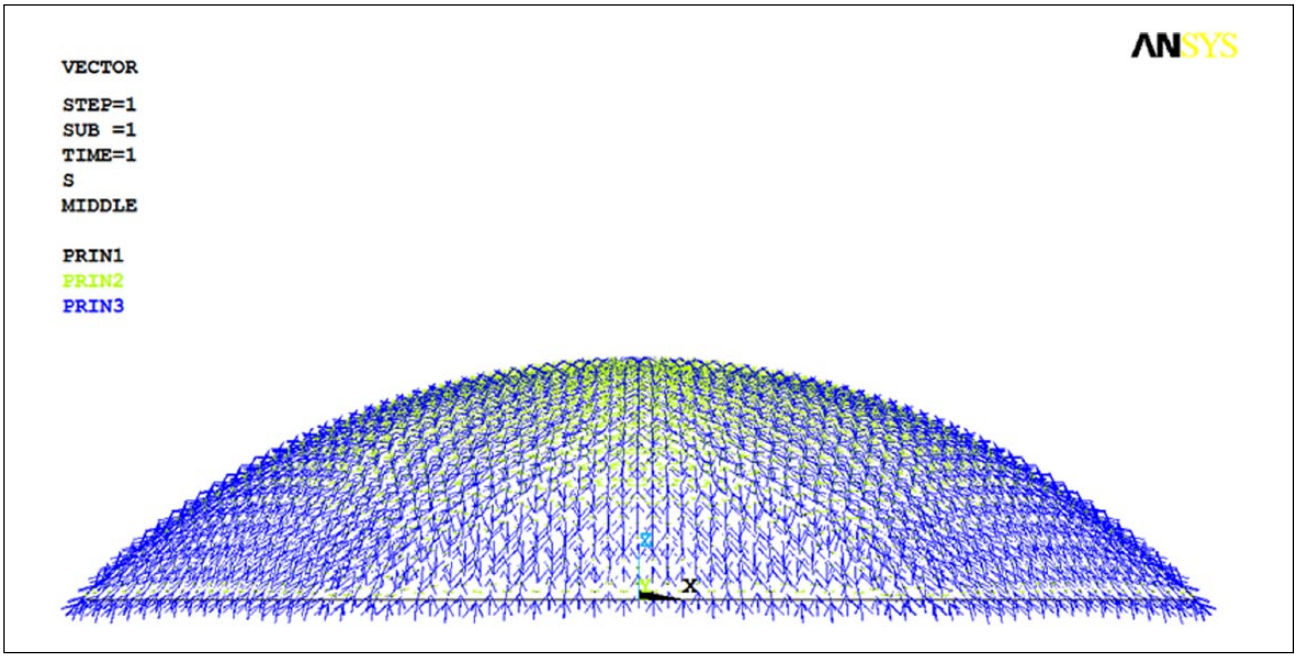

Figure 40. Vectorial representation of the principal stresses of the shell of *Example 3* (lateral view).

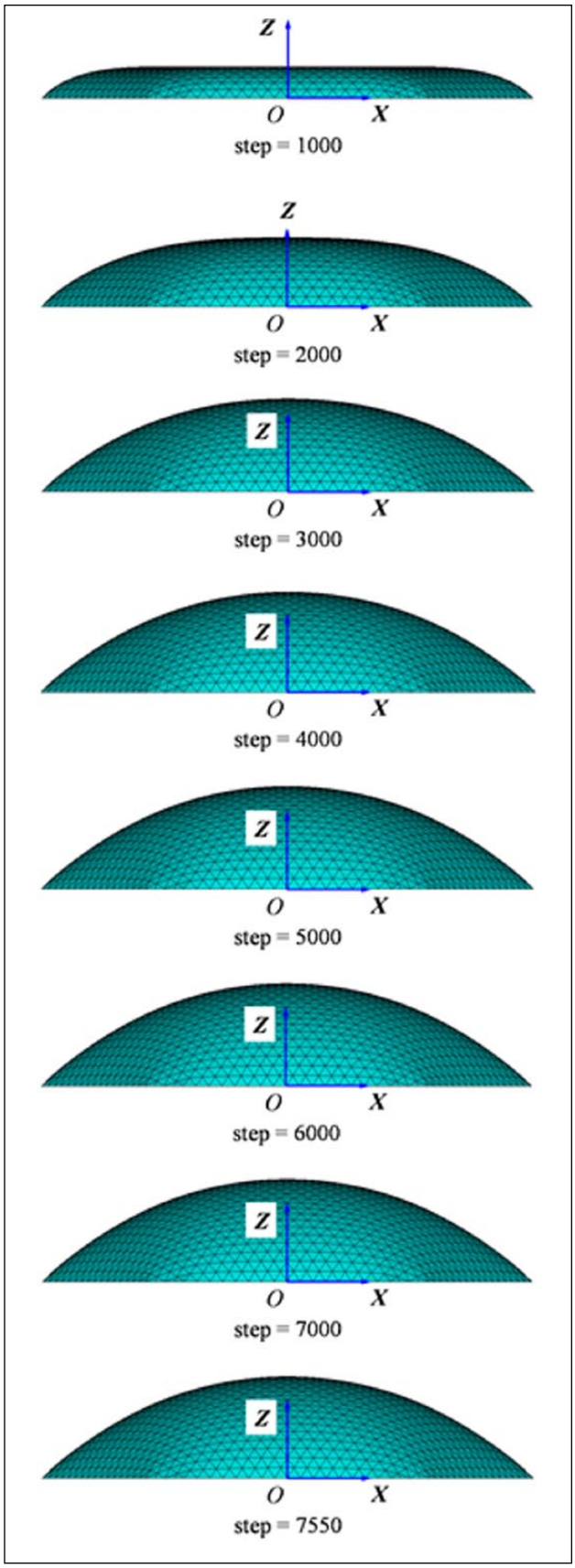

Figure 41. Inflation process of the pneumatic model of *Example 3*.

In conclusion, VFIFE is a relatively new and promising method; it is successfully applied in form-finding problems of membrane structures and thus shells, which provides the researchers and designers with a new option to do relevant research.

Declaration of conflicting interests

The author(s) declared no potential conflicts of interest with respect to the research, authorship, and/or publication of this article.

Funding

The author(s) disclosed receipt of the following financial support for the research, authorship, and/or publication of this article: The work has been supported by the National Natural Science Foundation of China (Grant No. 51378150 and Grant No. 51578186).

References

1. Chilton J. *The Engineer's contribution to contemporary architecture: Heinz Isler*. London: Thomas Telford Publishing, 2000.
2. Ramm E. Heinz Isler shells – the priority of form. *J Int Assoc Shell Spat Struct* 2011; 52(3): 143–154.
3. Nerdinger W, With IC, Meissner I, et al. (eds) *Frei Otto complete works: lightweight construction, natural design*. Beijing, China: China Architecture & Building Press, 2010.
4. Nicoletti M. *Sergio Musmeci, Organicità di forme e forze nello spazio*. Turin: Testo & Immagine, 1999.
5. Bini D. *Building with air*. London: Bibliotheque McLean, 2014.
6. Kokawa T. Building techniques for ice shell as temporary structure. In: *Proceedings of IASS-APCS: From spatial structures to space structures*, Seoul, Korea, 21–24 May 2012.
7. Day AS. An introduction to dynamic relaxation. *Engineer* 1965; 29(2): 218–221.
8. Linkwitz K and Schek HJ. Einige Bemerkungen zur Berechnung von vorgespannten Seilnetzkonstruktionen. *Ing Arch* 1971; 40: 145–158.
9. Schek HJ. The force density method for form-finding and computations of general networks. *Comput Method Appl M* 1974; 3: 115–134.
10. Haug E and Powell GH. Finite element analysis of nonlinear membrane structures. In: *Proceedings of the IASS Pacific symposium part II: on tension structures and space frames*, Tokyo and Kyoto, Japan, 1972, pp. 93–102.
11. Bletzinger K-U and Ramm E. Form finding of shells by structural optimization. *Eng Comput* 1993; 9: 27–35.
12. Ting EC, Shih C and Wang YK. Fundamentals of a vector form intrinsic finite element: part I. Basic procedure and a plane frame element. *J Mech* 2004; 20(2): 113–122.
13. Ting EC, Shih C and Wang YK. Fundamentals of a vector form intrinsic finite element, part II: plane solid elements. *J Mech* 2004; 20(2): 123–132.
14. Shih C, Wang YK and Ting EC. Fundamentals of a vector form intrinsic finite element, part III: convected material frame and examples. *J Mech* 2004; 20(2): 133–143.

15. Block P and Ochsendorf J. Thrust network analysis: a new methodology for three dimensional equilibrium. *J Int Assoc Shell Spat Struct* 2007; 48(3): 167–173.
16. Vizotto I. Computational generation of free-form shells in architectural design and civil engineering. *Automat Constr* 2010; 19: 1087–1105.
17. Veenendaal D and Block P. An overview and comparison of structural form finding methods for general networks. *Int J Solids Struct* 2012; 49(26): 3741–3753.
18. Adriaenssens S, Block P, Veenendaal D, et al. (eds) *Shell structures for architecture: form-finding and optimization*. London: Routledge, 2014.
19. Wu TY and Ting EC. Large deflection analysis of 3D membrane structures by a 4-particle quadrilateral intrinsic element. *Thin Wall Struct* 2008; 46: 261–275.
20. Lien KH, Chiou YJ, Wang RZ, et al. Vector Form Intrinsic Finite Element analysis of nonlinear behavior of steel structures exposed to fire. *Eng Struct* 2010; 32: 80–92.
21. Wang RZ, Tsai KC and Lin BZ. Extremely large displacement dynamic analysis of elastic-plastic plane frames. *Earthquake Eng Struc* 2011; 40: 1515–1533.
22. Wu TY. Dynamic nonlinear analysis of shell structures using a Vector Form Intrinsic Finite Element. *Eng Struct* 2013; 56: 2028–2040.
23. Zhao Y, Wang Z and Peng T. Membrane element based on Vector Form Intrinsic Finite Element and its application in wrinkling analysis of membrane structures. *J Build Struct* 2015; 36(1): 127–135 (in Chinese).
24. Luo Y, Zheng Y and Yang C. Review of the finite particle method for complex behaviors of structures. *Eng Mech* 2014; 31(8): 1–7 (in Chinese).
25. Yang C, Shen Y and Luo Y. An efficient numerical shape analysis for light weight membrane structures. *J Zhejiang Univ: Sc A* 2014; 15(4): 255–271.
26. Wang Z. *Theory and application of thin shell element based on the Vector Form Intrinsic Finite Element method*. PhD Thesis, Zhejiang University, Hangzhou, China, 2013.